高等学校化学学报
CHEMICAL JOURNAL OF CHINESE UNIVERSITIES
综合评述

卤化物固态电解质制备工艺研究进展：从实验室合成到规模化制造

张桢溥[1,3]，洪博龙[3]，杨道通[1,3]，倪海津[2,3]，黄科科[1]，韩松柏[3]

（1. 吉林大学化学学院，无机合成与制备化学全国重点实验室，长春 130012；
2. 北京大学深圳研究生院新材料学院，深圳 518055；
3. 南方科技大学，深圳市固态电池研发重点实验室，广东省电驱动力能源材料重点实验室，粤港澳光热电能源材料与器件联合实验室，新材料重大科技设施研究院，前沿与交叉科学研究院，深圳 518055）

摘要 卤化物固态电解质因具有较好的氧化稳定性、较高的离子电导率和良好的机械可加工性，近年来成为全固态电池领域的重要研究方向. 随着氯化物以及氧氯化物、氮氯化物等体系的发展，卤化物固态电解质在离子传输性能和结构调控方面取得了显著进展. 然而，此类材料目前仍主要停留在实验室小批量制备和电池验证阶段，其规模化应用仍面临诸多问题. 本文综合评述了机械球磨法、固相反应法、溶液法、气相沉积法及相关复合工艺等主要制备方法，比较了不同工艺在结构调控和规模化制备潜力等方面的特点，并进一步分析了卤化物固态电解质由实验室制备走向规模化制造过程中待解决的问题，包括批次一致性控制、制造成本降低、环境稳定性提升、工艺过程可控性以及与实际电池制造的适配，以期为卤化物固态电解质的工艺优化、规模化制备及其在全固态电池中的应用研究提供参考.

关键词 卤化物固态电解质；全固态电池；制备工艺；规模化制备

中图分类号 O613；O646　　**文献标志码** A　　doi：10.7503/cjcu20260203

Preparation Strategies of Halide Solid-State Electrolytes: From Laboratory Synthesis to Scalable Manufacturing

ZHANG Zhenpu[1,3], HONG Bolong[3], YANG Daotong[1,3], NI Haijin[2,3], HUANG Keke[1*], HAN Songbai[3*]

(*1. State Key Laboratory of Inorganic Synthesis and Preparative Chemistry, College of Chemistry, Jilin University, Changchun* 130012, *China*;
2. School of Advanced Materials, Peking University Shenzhen Graduate School, Shenzhen 518055, *China*;
3. Shenzhen Key Laboratory of Solid State Batteries, Guangdong Provincial Key Laboratory of Energy Materials for

收稿日期：2026-05-16. 网络首发日期：2026-06-29.

联系人简介：黄科科，男，博士，教授，主要从事无机固体化学方面的研究. E-mail：kkhuang@jlu.edu.cn
韩松柏，男，博士，教授，主要从事中子表征技术与能源材料方面的研究. E-mail：hansb@sustech.edu.cn

基金项目：吉林省科技发展计划项目（批准号：YDZJ202501ZYTS291, 20260602013RC）、长春市科技发展计划项目（批准号：2024GZZ02）、广东省资助项目（批准号：2021ZT09C064）、国家自然科学基金（批准号：12275119, 52227802, 12426301, 525B2028）、广东省基础与应用基础研究基金（批准号：2024B1515120042）、深圳市科技计划项目（批准号：KQTD20200820113047086）、深圳市固态电池研发重点实验室（批准号：SYSPG20241211173726011）、粤港澳光热电能源材料与器件联合实验室（批准号：2019B121205001）和广东省电驱动力能源材料重点实验室（批准号：2018B030322001）资助.

Supported by the Jilin Province Science and Technology Development Plan Project, China(Nos. YDZJ202501ZYTS291, 20260602013RC), the Science and Technology Development Plan Project of Changchun, China(No. 2024GZZ02), the Guangdong Grants(No. 2021ZT09C064), the National Natural Science Foundation of China(Nos. 12275119, 52227802, 12426301, 525B2028), the Guangdong Basic and Applied Basic Research Foundation, China(No. 2024B1515120042), the Shenzhen Science and Technology Program, China(No. KQTD20200820113047086), the Shenzhen Key Laboratory of Solid State Batteries, China(No. SYSPG20241211173726011), the Guangdong-Hong Kong-Macao Joint Laboratory for Photonic-Thermal-Electrical Energy Materials and Devices, China(No. 2019B121205001) and the Guangdong Provincial Key Laboratory of Energy Materials for Electric Power, China(No. 2018B030322001).

Electric Power, *Guangdong-Hong Kong-Macao Joint Laboratory for Photonic-Thermal-Electrical Energy Materials and Devices*, *Institute of Major Scientific Facilities for New Materials*, *Academy for Advanced Interdisciplinary Studies*, *Southern University of Science and Technology*, *Shenzhen* 518055, *China*)

Abstract Owing to their favorable oxidative stability, high ionic conductivity, and good mechanical processability, halide solid-state electrolytes have emerged as promising electrolyte candidates for all-solid-state batteries. With the development of systems such as chlorides, oxychlorides, and nitride-chlorides, halide solid-state electrolytes have made significant progress in ionic transport performance and structural regulation. However, these materials are still mainly at the stage of laboratory-scale preparation and cell validation, and their scalable application still faces several issues. This review summarizes the major preparation methods, including ball milling, solid-state reaction, solution-based synthesis, vapor-phase deposition, and related hybrid processing strategies. The characteristics of different processes in terms of structural regulation and scalable preparation potential are compared, and the key issues that need to be addressed during the transition from laboratory preparation to scalable manufacturing are further analyzed, including batch-to-batch consistency control, manufacturing-cost reduction, environmental-stability improvement, process controllability, and compatibility with practical battery-manufacturing workflows, thereby providing a reference for process optimization, scalable preparation, and application research of halide solid-state electrolytes in all-solid-state batteries.

Keywords Halide solid-state electrolyte; All-solid-state battery; Preparation strategy; Scalable preparation

1 Introduction

With the rapid development of renewable-energy integration, electric transportation, and portable electronic devices, secondary batteries are required to deliver higher energy density, improved safety, longer cycle life, and controllable cost[1—4]. Conventional lithium-ion batteries rely on flammable organic liquid electrolytes, which may suffer from leakage, combustion, and thermal runaway under high-temperature, overcharge, mechanical abuse, or high-voltage operating conditions. In addition, side reactions between liquid electrolytes and high-energy-density electrodes such as Ni-rich cathodes and Li-metal anodes can limit long-term cycling stability[5—8]. Therefore, all-solid-state batteries, in which liquid electrolytes are replaced by solid-state electrolytes, are regarded as an important route to improve intrinsic battery safety and further increase energy density[9—14].

In all-solid-state batteries, solid-state electrolytes (SSEs) not only serve as ion-conducting and electron-blocking components, but also directly influence electrode/electrolyte interfacial stability, composite-electrode construction, rate capability, and cycle life[15—19]. The most widely studied inorganic SSEs include oxides, sulfides, and halides. Oxide solid electrolytes generally exhibit good chemical stability and mechanical strength, but usually require high-temperature sintering and suffer from large solid-solid interfacial resistance[20—22]. Sulfide solid electrolytes show high ionic conductivity (up to 10^{-2} S/cm) and good cold-pressing processability, but their air stability and compatibility with high-voltage cathodes still need improvement[23—25]. In comparison, halide SSEs combine high oxidative stability, favorable interfacial compatibility with high-voltage cathodes, and certain mechanical compressibility, giving them distinctive advantages of high-voltage all-solid-state batteries[26—30].

The research foundation of halide SSEs can be traced back to early studies on lithium halides and multicomponent halide ion conductors. However, their emergence as a research hotspot for all-solid-state batteries was mainly driven by high-performance systems such as Li_3YCl_6, Li_3YBr_6, and Li_3InCl_6[31,32]. These materials demonstrated that halides can not only achieve ionic conductivities on the order of 10^{-3} S/cm, but also show good interfacial compatibility with high-voltage oxide cathodes[31—34]. Subsequently, researchers

have optimized ion transport in halides through anion stacking, cation disorder, aliovalent doping, mixed-halide regulation, and local structural design, gradually forming multi-anion material systems represented by pure halides, oxyhalides, and nitride-halides[35—38].

Although halide SSEs have prominent advantages in matching high-voltage cathodes, their practical application still faces several challenges, including the reliance of some high-performance systems on costly rare-earth elements, sensitivity to moisture, limited reductive stability against Li-metal anodes, difficulties in constructing intimate interfaces and continuous ion-transport networks in composite electrodes, and immature scalable preparation technologies[26—30]. Therefore, the development of halide SSEs should not focus only on improving ionic conductivity, but should also consider material composition, local structure, preparation route, environmental stability, interface engineering, and industrial scale-up. On this basis, this review summarizes the material systems and structural features of pure halides, oxyhalides, and nitride-halides, and then discusses the application characteristics of ball milling, solid-state reaction, solution synthesis, vapor-phase deposition, and other hybrid processes in preparing halide SSEs(Fig.1). Furthermore, the differences among these routes in structural regulation, environmental sensitivity, and scale-up potential are compared. Furthermore, new material development, process scale-up, *in situ* characterization, data-driven optimization, and commercialization progress are discussed to identify key issues in the transition of halide SSEs from laboratory-scale synthesis to scalable manufacturing, followed by perspectives on future development.

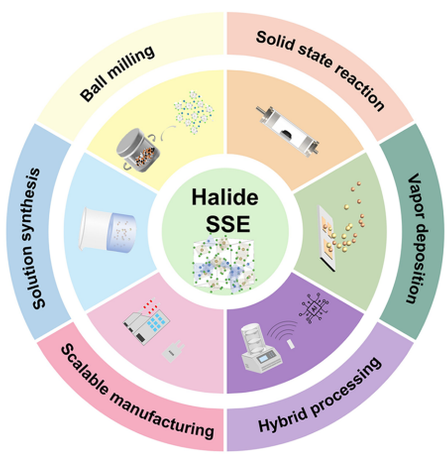


Fig. 1 Schematic illustration of representative preparation and scale-up pathways for halide SSEs

2 Structure and Ion-Transport Mechanisms of Halide Solid-State Electrolytes

The study of halide SSEs can be traced back to investigations of ionic conduction in metal halides in the 1930s. As early as 1930, Ginnings and Phipps[39] systematically studied the relationship between temperature and conductivity for solid lithium halides such as LiF, LiCl, LiBr, and LiI. However, these early simple halides generally showed low ionic conductivity, and related studies remained focused for a long time on defect diffusion, temperature-dependent conductivity, and fundamental solid-state ionics, far from meeting the requirements of practical all-solid-state batteries[39,40]. A key turning point came in 2018, when Asano *et al.* reported Li_3YCl_6 and Li_3YBr_6 with ionic conductivities on the order of 10^{-3} S/cm, good densification behavior, and compatibility with 4 V-class cathodes, marking the transition of halides from basic ion conductors to high-performance solid electrolytes for all-solid-state batteries[31].

Subsequently, a series of high-performance halide SSEs, such as Li_3InCl_6, Li_3ScCl_6, and Li_2ZrCl_6, were developed, and research rapidly expanded to systems with different metal cations, halide anions, and local structural regulation strategies[32,41—43]. In general, high-performance halide SSEs can be described by a Li-M-X framework, where M can be Sc, Y, La, In, Zr, Ta, Ti, V, Cr, Mn, Fe, Co, Ni, and other metal elements, while X mainly includes F, Cl, Br, and I[37,44,45]. By regulating the valence state and ionic radius of the metal cation, anion stacking, Li^+ site occupancy, and vacancy concentration, the Li^+ migration pathways and ionic conductivity in the halide framework can be effectively tuned.

With deeper research, the evaluation criteria for halide SSEs have gradually expanded from ionic

conductivity alone to air stability, mechanical processability, interfacial compatibility, raw-material cost, and scale-up potential[37,44—46]. Therefore, beyond conventional pure halides, researchers have introduced non-halide anions such as O^{2-} and N^{3-} to construct oxyhalide and nitride-halide systems, enabling the coupled regulation of local coordination environments, structural disorder, amorphization behavior, and interfacial stability[47—49]. According to anion chemistry, this review divides halide SSEs into pure halides, oxyhalides, and nitride-halides, and discusses their development, structural features, and performance-regulation mechanisms.

2.1 Halides

Halide SSEs refer to inorganic lithium-ion conductors in which halide anions constitute the main framework. They can generally be described by the $Li_aM_bX_c$ structure, where M represents a metal element and X represents F, Cl, Br, or I. Compared with oxide and sulfide SSEs, pure halides usually exhibit higher compatibility with high-voltage cathodes and better cold-pressing behavior, making them important cathode-side electrolytes for all-solid-state batteries[31,32,37,44]. Structurally, these materials are typically based on close-packed halide-anion frameworks, with Li^+ and high-valence metal cations occupying octahedral or tetrahedral interstices. Their ion-transport behavior is collectively governed by anion stacking, Li-site occupancy, vacancy concentration, cation disorder, and local lattice softness[36,37,44,50].

As shown in Fig. 2(A) and (B), pure halide SSEs can generally be classified into hcp and ccp types according to the stacking mode of the anion sublattice. In hcp-type structures, halide anions usually follow an A-B-A-B stacking sequence. Representative systems include Li_3YCl_6, Li_3ErCl_6, and some rare-earth chlorides, in which Li^+ and M^{3+} mainly occupy octahedral sites, and the ion-transport pathways are closely related to layered stacking, cation disorder, and stacking faults[31,50,51]. In ccp-type structures, the anion sublattice typically follows an A-B-C-A-B-C stacking sequence. Representative systems include Li_3YBr_6, Li_3InCl_6, $Li_2Sc_{2/3}Cl_4$, and some In/Zr/Hf-based chlorides, where Li^+ can form more continuous three-dimensional migration networks between octahedral and tetrahedral sites[31,32,36,52]. The layered structure of Li_3InCl_6 further illustrates the typical ccp-type framework of In-based chloride electrolytes, as shown in Fig. 2(C)[32]. In addition, the study of $Li_3Y_{1-x}In_xCl_6$ showed that increasing the In^{3+} content can induce a

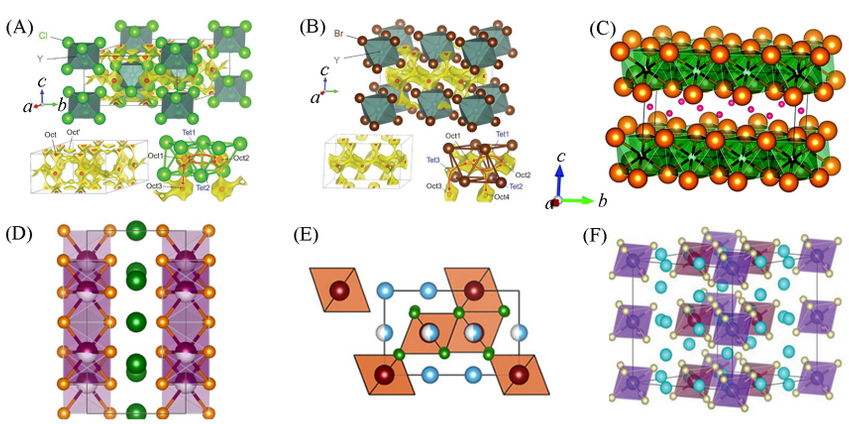


Fig. 2 Representative crystal structures, Li^+ migration pathways, and structural regulation mechanisms of pure halide SSEs

(A, B) Rietveld-refined crystal structures of Li_3YCl_6 and Li_3YBr_6 overlaid with BVSE-calculated Li^+ potential maps[31]; (C) layered structure of Li_3InCl_6[32]; (D) schematic illustration of composition-induced structural evolution in $Li_3Y_{1-x}In_xCl_6$[36]; (E) schematic representation of a typical stacking fault in Li_3YCl_6[50]; (F) DFT-calculated defect model of Li_3ErCl_6, showing cation-site disorder associated with Er-site occupancy[51].

(A, B) Copyright 2018, Wiley-VCH; (C) Copyright 2019, the Royal Society of Chemistry; (D) Copyright 2020, Wiley-VCH; (E) Copyright 2022, American Chemical Society; (F) Copyright 2020, Wiley-VCH.

transition of the anion framework from hcp to ccp, and the ccp anion sublattice generally corresponds to faster Li^+ migration, as shown in Fig.2(D)[36].

Beyond the average crystal structure, local defects and structural disorder are also important origins of high ionic conductivity in pure halides. As shown in Fig.2(E), Sebti *et al.*[50] used neutron diffraction and simulations to reveal a high concentration of defects in Li_3YCl_6 and showed that the concentration of stacking faults can be tuned by synthesis and heat-treatment conditions, thereby affecting Li^+ migration. Similarly, the DFT-calculated defect model of Li_3ErCl_6 in Fig.2(F) shows that different Er-site occupation/disorder configurations can affect local structural stability[51]. These results indicate that the high conductivity of pure halides originates not only from diffusion channels in ideal crystal structures, but also from stacking faults, site disorder, and local distortions introduced by nonequilibrium synthesis.

In recent years, structural regulation of pure halides has expanded from single-composition systems to multi-cation, aliovalent-doping, and mixed-halide designs. $Li_3Y_{1-x}In_xCl_6$ realizes hcp-ccp framework regulation through Y/In mixed cations and significantly improves humidity tolerance[36]. $Li_{3-x}In_{1-x}Hf_xCl_6$ introduces Li vacancies through aliovalent substitution of In^{3+} by Hf^{4+}, improving ionic conductivity while maintaining electrochemical stability; among these compositions, $Li_{2.7}In_{0.7}Hf_{0.3}Cl_6$ reaches a conductivity of 1.28 mS/cm[53]. These studies show that the essence of aliovalent doping is to regulate Li vacancies or interstitial sites through charge compensation, thereby optimizing carrier concentration and migration pathways.

Mixed-halide design provides another route to tune the softness and dynamic behavior of the anion framework. Liu *et al.*[54] found that the superionic transition of Li_3YCl_6 is closely related to collective anion motion. By using Cl/Br mixing to reduce the superionic transition temperature, $Li_3YCl_{4.5}Br_{1.5}$ and $Li_3GdCl_3Br_3$ achieved ionic conductivities of 6.1 and 11 mS/cm, respectively. This result indicates that halide anions are not merely static frameworks; their collective vibrations, polarizability, and local dynamic rearrangements may participate in Li migration. Overall, pure halide SSEs have evolved from initial single-composition systems such as Li_3YCl_6 and Li_3YBr_6 toward a structural-engineering stage involving multi-cation, mixed-halide, aliovalent-doping, and defect-regulation strategies. In the future, balancing high ionic conductivity, high-voltage stability, air stability, and low cost will remain a key issue for the continued development of pure halides.

2.2 Oxyhalides

As research on pure halide SSEs has progressed, it has become clear that conventional rare-earth halide systems, although possessing high ionic conductivity and good cathode compatibility, still suffer from the high cost of some metal elements, mechanical brittleness, insufficient air stability, and high costs for scalable preparation[47,55,56]. Therefore, researchers have attempted to introduce O^{2-} into halide frameworks to construct oxyhalide SSEs, aiming to preserve the high-voltage stability and densification capability of halides while using oxide anions to regulate local coordination environments, structural disorder, and interfacial chemistry[55,56].

In 2023, Zhang *et al.*[47] reported an amorphous oxychloride solid-electrolyte family, xLi_2O-MCl_y (M=Ta, Hf)[Fig.3(A)], providing an important starting point for the development of oxyhalides. This work demonstrated that introducing Li_2O into metal chlorides can effectively disrupt the long-range order of conventional halide lattices and form highly locally disordered amorphous Li-M-O-Cl networks. The optimized $1.6Li_2O$-$TaCl_5$ showed a ionic conductivity of 6.6×10^{-3} S/cm, good cold-pressing behavior, a broad composition window, and long-term cycling stability; all-solid-state batteries based on this electrolyte could operate for more than 2400 cycles. These results indicate that oxyhalides are not simply halides with oxygen

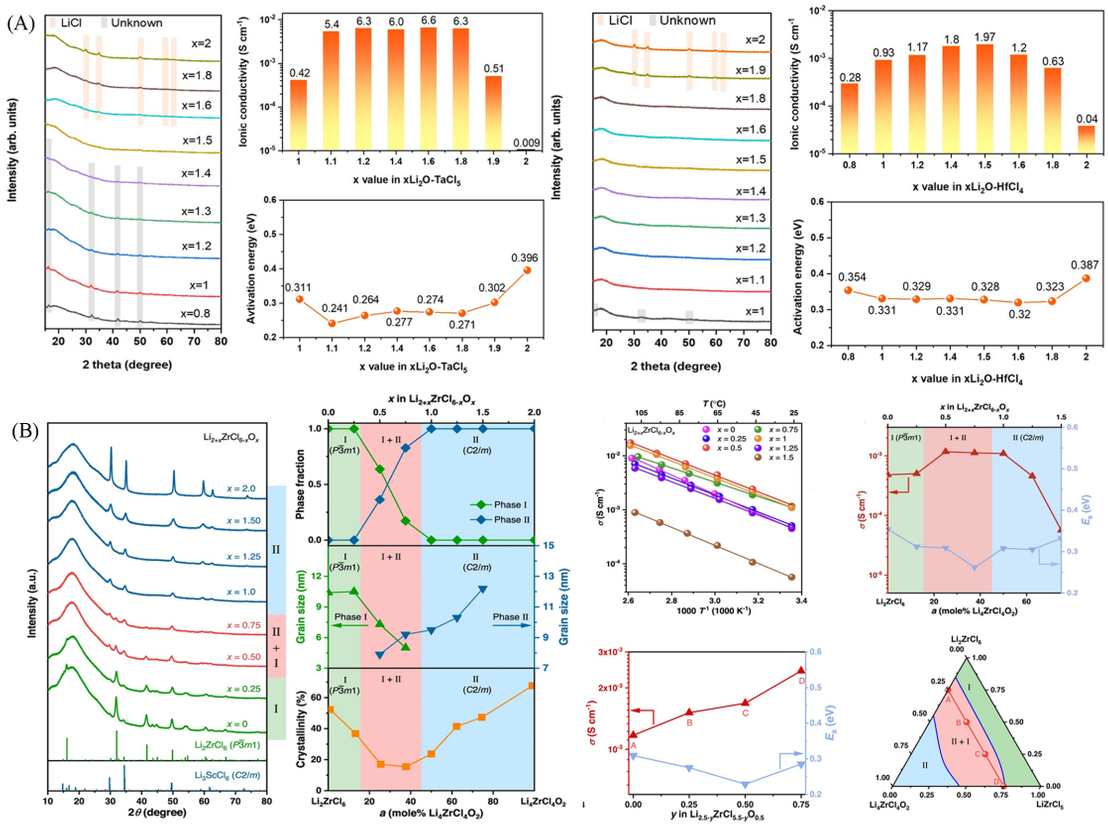


Fig. 3 Structural evolution and ion-transport properties of representative oxyhalide SSEs

(A) Laboratory XRD patterns, ionic conductivities and activation energies of amorphous $x$$Li_2O$-$TaCl_5$ and $x$$Li_2O$-$HfCl_4$ SSEs[47]; (B) composition-dependent phase evolution and ion-transport properties of Zr-based oxychloride SSEs[55].

(A) Copyright 2023, Springer Nature; (B) Copyright 2023, Springer Nature.

incorporated, but can use oxygen-induced amorphization to construct new disordered ion-transport networks, enabling high ionic conductivity under relatively low-temperature and mild processing conditions.

Almost simultaneously, Hu *et al.*[55] reported a low-cost and compressible $Li_{1.75}ZrCl_{4.75}O_{0.5}$ oxychloride solid electrolyte [Fig.3(B)], further advancing oxyhalides toward rare-earth-free and low-cost systems. This material exhibited an ionic conductivity of 2.42 mS/cm at 25 ℃, a relative density of 94.2% under 300 MPa, and an estimated raw-material cost of only about 11.60 USD/kg. Compared with conventional Y-, Sc-, and In-based high-cost halide systems, Zr-based oxychlorides simultaneously possess high ionic conductivity, compressibility, and cost advantages, indicating that oxyhalides are not only a structural-regulation strategy but may also provide an effective route to reduce raw-material cost and improve mechanical processability.

In addition, the viscoelastic inorganic glass electrolyte $LiAlCl_{2.5}O_{0.75}$ proposed by Dai *et al.*[56] further demonstrated the possibility of developing oxyhalides into "soft inorganic electrolytes". By introducing oxygen into $MAlCl_4$-type chloroaluminates, this class of materials forms inorganic glass systems with polymer-like viscoelasticity. $LiAlCl_{2.5}O_{0.75}$ combines a ionic conductivity of >1 mS/cm, good oxidative stability, and remarkable deformability, enabling stable solid-solid interfacial contact under low stack pressure. This work suggests that oxyhalides can not only enhance ion conduction through amorphization and soft-lattice structures, but also alleviate the persistent problems of interfacial contact and mechanical mismatch in solid-state batteries through viscoelastic inorganic-glass design.

2.3 Nitride-Halides

As halide solid-state electrolyte research has moved from crystalline structural design toward amorphization and multi-anion regulation, researchers have attempted to introduce N^{3-} to construct

nitride-halide/nitride-chloride solid electrolyte systems. Compared with O^{2-}, N^{3-} has a higher charge density and stronger bridging ability, which can more strongly disrupt the long-range order of metal chlorides and induce reconstruction of local coordination polyhedra, thereby establishing amorphous ion-transport networks. This has become one of the most frontier directions in halide SSEs[48,57—59].

As shown in Fig.4(A), the preparation route and structural characterization reported by Hong *et al.*[48] demonstrate that amorphous $Li_{3x}MCl_yN_x$ (M=Ta or La) nitride-halide SSEs can be constructed through a nitrogen-assisted amorphization strategy. Using Li_3N and metal chlorides as precursors, this work showed that high-energy ball milling can introduce dual-anion amorphous networks and eliminate obvious long-range crystalline order in both Ta- and La-based nitride-halides. Among them, Ta-based $Li_{3x}TaCl_5N_x$ delivered a maximum ionic conductivity of 7.34 mS/cm at 30 ℃ and showed good battery compatibility under high-rate, high-voltage, and low-temperature conditions. These results show that nitride-halides can simultaneously improve ion transport and solid-solid interfacial contact through an amorphization strategy, providing an important direction for extending halide SSEs from crystalline framework design to amorphous network design.

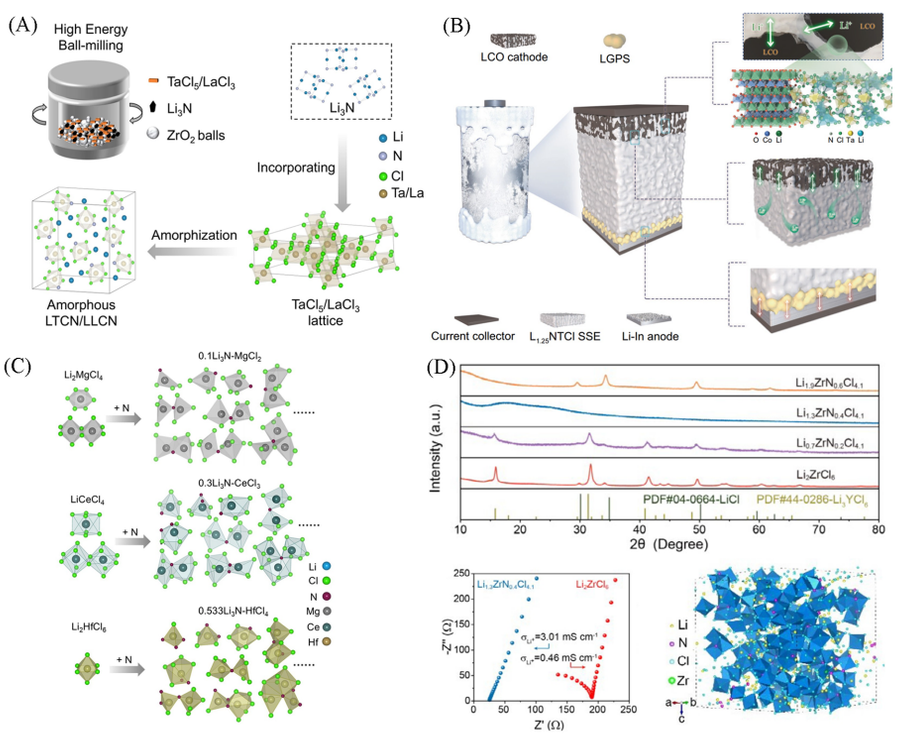


Fig. 4 Amorphization strategy, low-temperature battery design, and ion-transport properties of nitride-halide SSEs

(A) Schematic illustration of the preparation of amorphous LMCN nitride-halide solid electrolytes[48]; (B) schematic configuration of an all-solid-state battery designed for operation under extreme cold conditions[57]; (C) evolution of metal-centered coordination clusters from crystalline Li-M-Cl precursors to amorphous xLi_3N-MCl_y nitride-halide networks[49]; (D) XRD patterns of Li_2ZrCl_6 and $Li_{3x+0.1}ZrN_xCl_{4.1}$, Nyquist plots of $Li_{1.3}ZrN_{0.4}Cl_{4.1}$ and Li_2ZrCl_6, and MD-simulated structure of $Li_{1.3}ZrN_{0.4}Cl_{4.1}$[58].

(A) Copyright 2025, Wiley-VCH; (B) Copyright 2025, Springer Nature; (C) Copyright 2026, the Royal Society of Chemistry; (D) Copyright 2025, Wiley-VCH.

On this basis, Hong *et al.*[57] further developed amorphous xLi_3N-$TaCl_5$ nitride-chlorides for extremely low-temperature all-solid-state battery design. As illustrated in Fig.4(B), the amorphous electrolyte design enables continuous Li^+ migration pathways and avoids grain-boundary resistance, which is helpful for maintaining ion transport at low temperatures. The optimized electrolyte achieved an ionic conductivity of 5.91 mS/cm at 25 ℃. The assembled all-solid-state battery retained a discharge capacity of 137.6 mA·h/g

after 100 cycles at −30 ℃ and could operate continuously for more than 200 h at −60 ℃. This indicates that amorphous nitride-halide electrolytes not only exhibit high conductivity at room temperature, but also show application potential in low-temperature battery scenarios distinct from conventional crystalline halides.

Subsequently, Hong *et al.* [49] proposed a more general "nitrogen-induced amorphization" strategy and extended it from Ta/La systems to a broader range of metal chlorides. Fig. 4(C) highlights the structural evolution from crystalline Li-M-Cl precursors to amorphous $x\mathrm{Li_3N\text{-}MCl_y}$ ($0.3\leqslant 3x\leqslant 1.9$; $2\leqslant y\leqslant 4$) networks, revealing that N^{3-} can distort metal-centered coordination polyhedra, construct N-bridged networks, and disrupt long-range order. A representative $0.533\mathrm{Li_3N\text{-}HfCl_4}$ electrolyte achieved an ionic conductivity of 2.02 mS/cm at 25 ℃; all-solid-state batteries based on this electrolyte retained 81.87% of their capacity after 2000 cycles at 1000 mA/g and a high cathode loading of 6.24 mg/cm^2. This work indicates that nitride-halides have evolved from nitrogen doping to a designable amorphization strategy based on the high charge density and bridging ability of nitrogen.

Beyond Ta, La, and Hf-based systems, Zr-based nitride-halides also show strong development potential. As shown in Fig.4(D), the XRD, impedance and molecular dynamics results of $\mathrm{Li_{3x+0.1}ZrN_xCl_{4.1}}$ directly reveal the N^{3-} substitution-induced transformation from crystalline $\mathrm{Li_2ZrCl_6}$ to an amorphous nitride-chloride structure[58]. This structural transition significantly improves Li^+ transport, increasing the ionic conductivity from 0.46 mS/cm for pristine $\mathrm{Li_2ZrCl_6}$ to 3.01 mS/cm for $\mathrm{Li_{1.3}ZrN_{0.4}Cl_{4.1}}$. These results further confirm that nitrogen-induced amorphization is a general and effective approach for enhancing the conductivity of halide-derived SSEs.

3 Preparation Strategies of Halide Solid-State Electrolytes

3.1 Ball Milling

Ball milling synthesis is one of the most widely used routes for halide SSEs. Its basic principle is to trigger solid-state reactions under macroscopically low-temperature conditions through continuous collision, shear, and friction between milling balls and powders and between balls and the milling jar, while simultaneously introducing lattice distortion, site disorder, nanocrystallization, and amorphous structures. For halide systems, this method is particularly important because many high-performance halide electrolytes rely on a certain degree of structural disorder, cation mixing, or amorphous networks to achieve fast Li^+ migration. In addition, ball milling can reduce the risks of halide volatilization and high-temperature decomposition, making it one of the most representative preparation methods for current halide and derivative systems[31,32,36,60].

The $\mathrm{Li_3YCl_6}$ and $\mathrm{Li_3YBr_6}$ reported by Asano *et al.* [31] in 2018 demonstrated that halide SSEs can achieve ionic conductivities above 10^{-3} S/cm at room temperature, together with good compactability and high-voltage cathode compatibility. Subsequently, $\mathrm{Li_3InCl_6}$ was also shown to be obtainable through a mechanochemical route, reaching a ionic conductivity of 1.49×10^{-3} S/cm and exhibiting good air stability and high-voltage compatibility[32]. On this basis, ball milling was further extended to $\mathrm{Li_3YBr_6}$, $\mathrm{Li_3ErI_6}$, $\mathrm{Li_2ZrCl_6}$, $\mathrm{Li_3TiCl_6}$, and other systems[41,42,60,61]. In recent years, ball milling has also become an important preparation method for amorphous oxyhalides and nitride-halides. For example, Sun *et al.* [47] prepared amorphous $x\mathrm{Li_2O\text{-}MCl_y}$ (M=Ta, Hf) oxychlorides by one-step ball milling, among which $1.6\mathrm{Li_2O\text{-}TaCl_5}$ achieved a ionic conductivity of 6.6×10^{-3} S/cm. For nitride-halides, Hong *et al.* [48] reported amorphous $\mathrm{Li_{3x}MCl_yN_x}$ (M=Ta or La) solid electrolytes through high-energy ball milling of $\mathrm{Li_3N}$ and metal chlorides. Among them, Ta-based $\mathrm{Li_{3x}TaCl_5N_x}$ is denoted as LTCN. As shown in Fig.5, the PXRD patterns, impedance spectra, conductivity evolution and activation-energy analysis of LTCN under different ball-milling conditions demonstrate that nitrogen

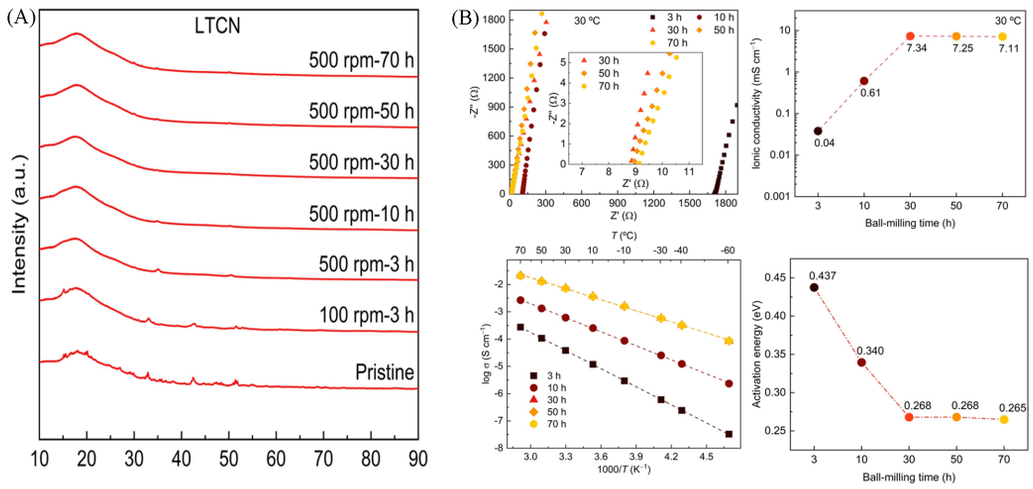


Fig. 5 Effect of ball-milling conditions on the structural evolution and ion-transport properties of amorphous $Li_{3x}TaCl_5N_x$ ($3x$=1.25) nitride-chloride solid electrolytes[48]

(A) PXRD patterns of LTCN prepared under different ball-milling conditions; (B) Nyquist plots, ionic conductivity evolution, Arrhenius conductivity plots, and corresponding activation energies of LTCN solid electrolytes with different milling times.

Copyright 2025, Wiley-VCH.

incorporation and milling-energy input jointly promote the formation of amorphous nitride-halide networks. The optimized LTCN ($3x$=1.25) achieved a high ionic conductivity of 7.34 mS/cm at 30 ℃, showing that ball milling can serve not only as a powder-mixing method, but also as an effective route for inducing amorphization and regulating Li^+ transport in dual-anion halide systems. In $0.533Li_3N$-$HfCl_4$, Hong *et al.*[49] further demonstrated that N^{3-} can act as a high-charge-density bridging anion to induce amorphization of various metal chlorides including $HfCl_4$, $ZrCl_4$, $CeCl_4$, $LaCl_4$, YCl_3, $MgCl_2$, and $MnCl_2$, indicating that nitrogen-induced amorphization has become an important direction for ball milling in halide-derived systems. Therefore, ball milling is no longer merely a conventional powder-mixing and solid-state reaction method, but has become an integrated preparation platform combining phase formation, defect regulation, amorphization design, and process screening.

The key parameters of ball milling include milling speed, milling time, ball-to-powder ratio, the materials of the milling balls and jar, atmosphere control, and post-treatment conditions. Most current studies use planetary ball mills, with common speeds concentrated in the range of 400—600 and 500 r/min being the most frequently used. Milling times are typically 10—70 h, and ball-to-powder ratios generally range from 20∶1 to 50∶1, with 40∶1 and 45∶1 being common values[32,47,48,57,60,62]. Because halide precursors are generally sensitive to moisture, milling is usually performed in an Ar-filled glovebox or sealed inert atmosphere, and ZrO_2 jars and balls are commonly used to reduce contamination. For crystalline Li_3MX_6 and Li_2MCl_6 systems, mild annealing is often required after milling to improve crystallinity and phase purity. For amorphous oxyhalides and nitride-halides, however, ball milling itself is often the key step for inducing amorphization and constructing ion-transport networks[47,48,57,60,62].

Taking representative systems as examples, Li_3InCl_6 is typically prepared by milling LiCl and $InCl_3$ in an Ar atmosphere using ZrO_2 jars and balls at 500 r/min for 24 h with a ball-to-powder ratio of 40∶1, followed by annealing at 260—400 ℃ for 2—12 h[32]. Li_3YBr_6 can be prepared by long-duration milling at 500 r/min for 50 h followed by annealing at 823 K for 2—24 h; the as-milled sample already shows a conductivity of 0.44×10^{-3} S/cm, which increases to 1.52×10^{-3} S/cm after annealing[60]. In amorphous multi-anion systems, $1.6Li_2O$-$TaCl_5$ forms an amorphous structure after premixing at 100 r/min for 2 h and high-speed milling at

500 r/min for 10 h[47]. $Li_{1.25}TaCl_5N_{0.42}$ achieves complete amorphization after premixing at 100 r/min for 3 h followed by 500 r/min milling for 30 h, with a conductivity of 7.34 mS/cm[48]. Therefore, the relationship between milling time and the degree of amorphization is especially important in nitride-halide systems.

As shown in Table 1, the role of ball milling differs among different halide systems. For crystalline or nanocrystalline halides such as Li_3InCl_6, Li_3YBr_6, Li_2ZrCl_6, and Li_3ScCl_6, ball milling mainly promotes solid-state reactions, refines particles, and introduces local disorder, while subsequent mild annealing improves phase purity and crystallinity[32,42,60,63]. For mixed-cation systems such as $Li_3Y_{1-x}In_xCl_6$, milling also promotes uniform cation mixing and is accompanied by a transition of the anion framework from hcp to ccp, thereby optimizing Li^+ migration pathways[36]. In contrast, for multi-anion systems such as xLi_2O-MCl_y and xLi_3N-MCl_y, ball milling directly drives amorphization; the introduction of O^{2-} or N^{3-} disrupts the long-range order of metal chlorides and forms continuous disordered networks with more open Li^+ diffusion pathways[47—49,57].

Table 1 Summary of ball-milling parameters for halide SSEs

Material	Structure	Conductivity/(S·cm^{-1})	Speed/(r·min^{-1})	Ball-to-powder ratio	Time/h	Post-treatment	Ref.
Li_3YCl_6	hcp/$P\bar{3}m1$	0.51×10^{-3}	500	—	50	—	[31]
Li_3YBr_6	ccp/$C2/m$	1.7×10^{-3}	500	—	50	Annealing at 550 ℃	[31]
Li_3InCl_6	ccp/$C2/m$	1.49×10^{-3}	500	40∶1	24	Annealing at 260 ℃, 5 h	[32]
Li_3YBr_6	ccp/$C2/m$	1.52×10^{-3}	500	—	50	Annealing at 823 K, 2 h	[60]
$Li_3Y_{1-x}In_xCl_6$	hcp/$P\bar{3}m1$	6.08×10^{-5}→	500	40∶1	36	Annealing at 260 ℃, 5 h	[36]
	→ccp/$C2/m$	1.42×10^{-3}					
Li_3ErI_6	Monoclinic/$C2/c$	0.65×10^{-3}	500	30∶1	83	—	[41]
Li_2ZrCl_6	hcp/$P\bar{3}m1$	4.46×10^{-4}	500	40∶1	36	Heat treatment at 100 ℃, 4 h	[42]
Li_3TiCl_6	Monoclinic/$C2/m$	1.04×10^{-3}	600	12∶1	24	Annealing at 300 ℃, 5 h	[61]
Li_3ScCl_6	Monoclinic/$C2/m$	1.01×10^{-3}	600	30∶1	10	Heated at 450 ℃, 30 min	[63]
$6Li_2O$-$TaCl_5$	Amorphous	6.6×10^{-3}	100+500	40∶1	2+10	—	[47]
$1.5Li_2O$-$HfCl_4$	Amorphous	1.97×10^{-3}	100+500	40∶1	2+10	—	[47]
$Li_{1.25}TaCl_5N_{0.42}$	Amorphous	7.34×10^{-3}	100+500	45∶1	3+30	—	[48]
$0.533Li_3N$-$HfCl_4$	Amorphous	2.02×10^{-3}	100+500	45∶1	3+30	—	[49]

Overall, ball milling has the advantages of low reaction temperature, broad applicability, and flexible parameter tuning. It enables rapid exploration of new compositions and can induce defects, stacking faults, nanocrystalline phases, or amorphous structures, making it especially suitable for rapid screening of halides, oxyhalides, and nitride-halides[31,32,36,47,49,57,60,62]. Its disadvantages include high sensitivity to precursor purity, environmental moisture, milling media, ball-to-powder ratio, and post-treatment conditions, while batch-to-batch consistency and manufacturing scale-up remain challenging. For example, a re-evaluation of Li_3YCl_6 showed that trace moisture below 500 mL/m^3 in YCl_3 can impair product purity, and water contents above 1% can reduce the conductivity by one to two orders of magnitude[64]. Therefore, the future focus of mechanochemical routes should not simply be "making the target phase", but rather advancing from experience-based experiments to reproducible, scalable, and industrially relevant process platforms through parameter optimization, orthogonal experiments, process monitoring, and data-driven methods[62,65].

3.2 Solid-State Reaction

The solid-state reaction is one of the most widely used routes in conventional inorganic material synthesis. Its basic principle is to mix the starting powders in stoichiometric proportions and then heat-treat them for an extended time, allowing Li^+, metal cations, and halide/oxyhalide anions to form the target crystalline phase through bulk diffusion, grain-boundary diffusion, or interfacial reactions. Compared with ball milling, the solid-state route relies more strongly on thermodynamic driving forces and long-range

diffusion, and is therefore more suitable for obtaining relatively highly crystalline standard samples with well-defined phase compositions. It is also useful for phase-stability studies, structural refinement, and metastable-phase capture[66—68]. However, because halides and oxyhalides are generally hygroscopic, prone to halogen volatilization, and often have narrow thermal-stability windows for certain precursors, solid-state routes usually require Ar atmospheres, vacuum-sealed tubes, sealed quartz ampoules, or dry environments, which differs markedly from the high-temperature sintering of conventional oxide ceramics in air[66—69].

In pure halide systems, Ito *et al.*[66] obtained nearly single-phase metastable β-Li_3YCl_6 by heating a mixed powder of LiCl and YCl_3 at 595 K for 50 h. This work further showed that both β-Li_3YCl_6 and α-Li_3YCl_6 have hcp-Cl^- anion frameworks, but differ in the arrangement of Li^+ and Y^{3+}. When the temperature exceeds 600 K, the system more readily transforms into the thermodynamically stable α-Li_3YCl_6, whereas long-term annealing at 595 K can kinetically stabilize the β phase[Fig.6(A)]. This indicates that solid-state reactions can not only form target crystalline phases, but also capture metastable superionic conductors through precise control of the temperature window.

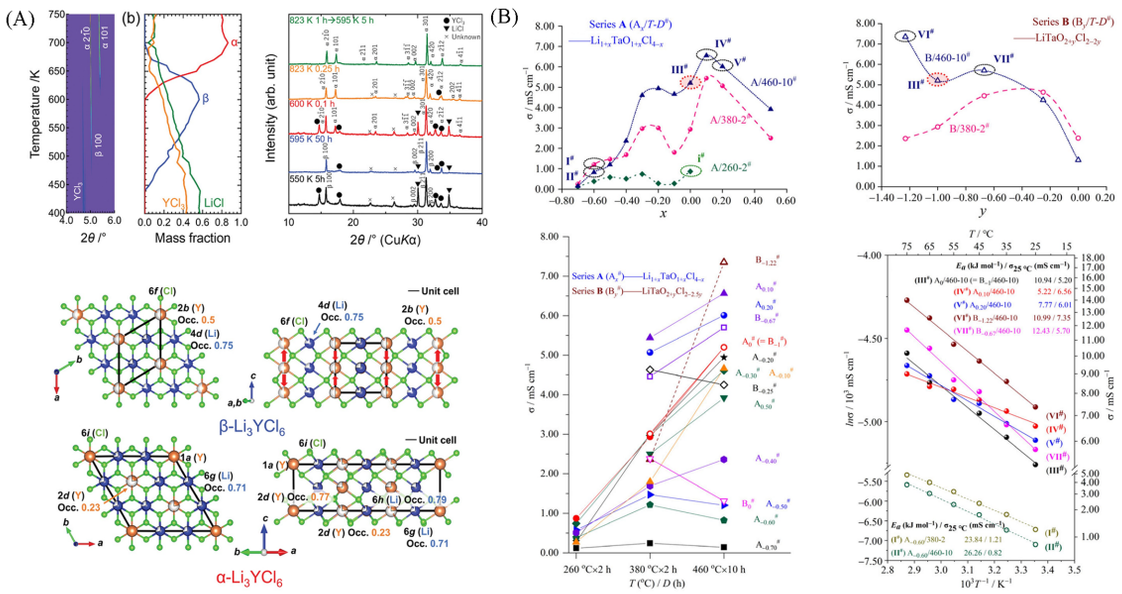


Fig. 6 Phase evolution and ion-transport properties of halide and oxyhalide solid electrolytes during solid-state reaction/annealing

(A) Characterization of Li_3YCl_6 formation from the solid-state reaction between LiCl and YCl_3, including temperature-dependent synchrotron XRD patterns, Rietveld-refined phase fractions, XRD patterns and crystal structures of β-Li_3YCl_6 and α-Li_3YCl_6[66]; (B) ionic conductivity evolution of crystalline Li—Ta—O—Cl as a function of composition, synthesis temperature and dwell time[71].

(A) Copyright 2021, Wiley-VCH; (B) Copyright 2025, MDPI.

For oxyhalides, Jeon *et al.*[70] prepared $LiNbOCl_4$ by low-temperature annealing using LiCl and $NbOCl_3$ as precursors, and the sample annealed at 125 ℃ reached a ionic conductivity of 8.4 mS/cm. This result suggests that, for some oxyhalides, low-temperature sealed annealing is sufficient to obtain highly conductive phases while avoiding corrosion and scale-up problems caused by HCl by-products. Li-Ta oxyhalides exhibit similar features. Bao *et al.*[71] used Li_2O, $TaCl_5$, and $LiTaO_3$ as precursors to prepare crystalline Li-Ta-O-Cl systems, including $Li_{1+x}TaO_{1+x}Cl_{4-x}$ and $LiTaO_{2+x}Cl_{2-2x}$, by reaction at 260—460 ℃ for 2—10 h[Fig.6(B)]. Among these, three-phase coexistence samples reached ionic conductivities of 5.20—7.35 mS/cm. In contrast, although earlier single-phase m-$LiTaOCl_4$ could be obtained by lower-temperature heat treatment, its conductivity was generally lower than that of multiphase samples, indicating that "phase purity" and "highest

ionic conductivity" are not always simply positively correlated in oxyhalides.

Overall, the solid-state route offers clear crystalline phases, strong structural interpretability, and relatively good batch reproducibility, making it particularly suitable for standard sample preparation, phase-diagram studies, metastable-phase capture, and structural confirmation of oxyhalides[66—72]. Its disadvantages include long reaction times, narrow temperature windows, strict requirements for sealing and atmosphere control, and the tendency of some halide precursors to volatilize or undergo side reactions during heating, leading to compositional deviations and impurity phases. Compared with ball milling, the solid-state route is less flexible for rapid screening and amorphization design.

3.3 Solution Synthesis

Solution synthesis is one of the most promising low-temperature, homogeneous, and scalable preparation routes for halide SSEs. Its basic concept is to dissolve LiCl and MCl_3, or related metal halide precursors, in water, alcohols, nitriles, ethers, or other solvents so that Li^+, metal cations, and halide anions are fully mixed at the molecular/ionic scale. The target electrolyte powders are then obtained through evaporation crystallization, precipitation, dehydration, or low-temperature annealing. Compared with ball milling, solution synthesis is more favorable for controlling nucleation, crystal growth, and particle morphology. Compared with the solid-state route, it usually requires lower reaction temperatures and more readily produces microstructures with homogeneous compositional distribution. Therefore, this method is considered an important route for moving halide SSEs from laboratory preparation toward scalable manufacturing[73—75].

In 2019, Li *et al.*[73] first reported a water-mediated synthesis route for Li_3InCl_6 [Fig. 7(A)]. In this work, LiCl and $InCl_3$ were dissolved in water to form a hydrated $Li_3InCl_6 \cdot 2H_2O$ intermediate, which was then

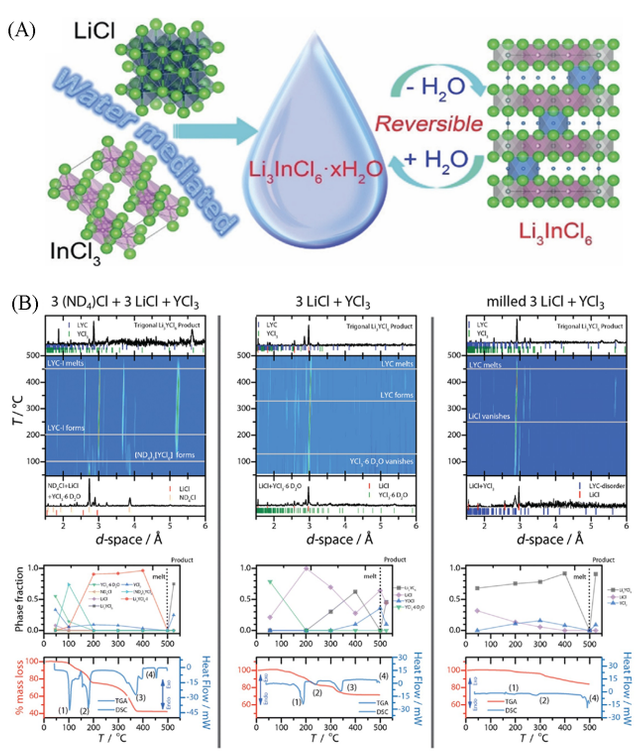


Fig. 7 Hydration/dehydration mechanism and intermediate-phase evolution during solution synthesis of halide SSEs

(A) Schematic illustration of water-mediated synthesis of Li_3InCl_6 through hydrated $Li_3InCl_6 \cdot xH_2O$ intermediates and reversible dehydration/rehydration[73]; (B) visualization of Li_3YCl_6 synthesis pathways using *in situ* neutron diffraction, phase-fraction analysis and TGA/DSC thermal analysis[75].

(A) Copyright 2019, Wiley-VCH; (B) Copyright 2024, the Royal Society of Chemistry.

dehydrated back to Li_3InCl_6, realizing a reversible hydration/dehydration transition between Li_3InCl_6 and $Li_3InCl_6 \cdot 2H_2O$. The resulting Li_3InCl_6 exhibited an ionic conductivity of 2.04×10^{-3} S/cm at 25 ℃. This result challenged the conventional view that halide SSEs cannot contact water and made Li_3InCl_6 one of the most representative systems for liquid-phase synthesis. Subsequently, Wang *et al.* [74] further used NH_4Cl-assisted halide intermediates to synthesize various Li_3MCl_6-type halide SSEs and showed that this method can regulate local structure and interfacial chemistry, converting the electrolyte/Li-metal interface from a mixed electron/ion-conducting interface into a more favorable Li^+-conducting interface. This indicates that solution synthesis is not only a low-temperature synthesis method, but can also participate in interface regulation and cell-structure design.

Nevertheless, the liquid-phase route cannot simply be applied to all halide systems. The ability of Li_3InCl_6 to be obtained through a hydration/dehydration route is mainly related to the hydrolysis behavior of In^{3+} and the stability of In-Cl coordination. In contrast, aqueous synthesis of Li_3YCl_6 relies more strongly on intermediate control. Brahmbhatt *et al.* [75] compared different synthesis routes for Li_3YCl_6 using *in situ* neutron diffraction [Fig. 7(B)] and found that, in the aqueous route, the formation of complex ammonium halide intermediates such as $(NH_4)_3YC_6$ is essential for Li_3YCl_6 crystallization. Without this intermediate, Y^{3+} is more likely to generate impurity phases such as YOCl through water coordination and hydrolysis. In that work, LiCl, YCl_3, and NH_4Cl were dissolved in water, followed by rotary evaporation, vacuum drying, and stepwise heating to 500 ℃ under Ar, systematically revealing the relationship among intermediates, local structure, and Li^+ migration during aqueous synthesis. This shows that the core of solution synthesis is not simply "dissolution and drying", but requires the design of solvents, intermediates, and desolvation pathways according to the water-coordination strength, hydrolysis tendency, and halide-complexing ability of metal cations.

Liu *et al.* [76] systematically compared the influence of different drying atmospheres after water-mediated synthesis of Li_3InCl_6. They found that wet precursors gradually heated to 200 ℃ under high vacuum produced less oxygen contamination and higher ionic conductivity. The ionic conductivities of the corresponding samples dried under high vacuum, low vacuum, Ar and N_2 were 2.70, 0.96, 0.39, and 0.22 mS/cm, respectively. This suggests that the key factor in aqueous synthesis is not simply whether water is used, but whether the dehydration process avoids oxide/oxychloride impurity formation while maintaining suitable particle morphology and grain-boundary structures. Wen *et al.* [77] further introduced HCl to regulate the water-mediated process and found that 5% (mass fraction) HCl can suppress Li_3InCl_6 decomposition and reduce LiCl impurities, giving a dehydrated sample with a conductivity of 2.76 mS/cm, which retained 2.38 mS/cm after exposure to 30% relative humidity air for 10 min. These results indicate that the core challenge of solution synthesis is not to completely avoid water or acid, but to suppress irreversible hydrolysis through controlled coordination environments and desolvation processes.

Beyond aqueous systems, organic solvents and aprotic solvents have gradually become important directions for liquid-phase synthesis of Li_3InCl_6. Bonsu *et al.* [78] systematically compared four solvent systems (THF, ACN, EtOH, and H_2O) and prepared Li_3InCl_6 *via* evaporation crystallization, vacuum drying at 80 ℃ for 45 min, and annealing at 200 ℃ for 2 h. The samples obtained using THF, ACN, EtOH, and H_2O exhibited ionic conductivities of 4.03, 3.67, 3.07, and 2.72 mS/cm, respectively, and the batch size could be scaled to 3—4 g. This study indicated that aprotic solvents help reduce microstrain and grain-boundary area, thereby enhancing ion transport and humidity stability. Xiong *et al.* [79] compared the effects of water, ethanol, and water-ethanol mixed solvents on the structure and properties of Li_3InCl_6 and found that ethanol-derived samples had larger lattice parameters, more Li^+ vacancies, and the highest conductivity of

1.06 mS/cm. Rosa *et al.*[80] further reported an ethanol-mediated route for preparing Li_3InCl_6. By dissolving precursors in absolute ethanol, evaporating overnight at 70 ℃, and annealing at 200 ℃ for 3 h under 10^{-2} Pa vacuum, phase-pure Li_3InCl_6 was obtained with a ionic conductivity of 0.73 mS/cm, good cold-press densification behavior, and interfacial stability.

Overall, solution synthesis has the advantages of low reaction temperature, homogeneous mixing of components, adjustable particle morphology, and easier integration with coating, infiltration, composite-cathode fabrication, and other battery-manufacturing processes[73—80]. Its disadvantages are that aqueous routes can readily introduce hydrates, oxides, or oxychloride impurities, while nonaqueous solvent routes impose higher requirements on solvent purity, anhydrous conditions, and solvent recovery. Moreover, the hydrolysis tendencies of different metal centers vary significantly, so the successful experience of Li_3InCl_6 cannot be directly extended to all halide systems such as Li_3YCl_6 and Li_3ScCl_6[75—77]. In the future, solution synthesis should evolve from "finding soluble solvents" toward solvated-structure design, intermediate control, dehydration-process regulation, and continuous scale-up, so as to establish liquid-phase preparation processes that are reproducible, scalable, and capable of delivering high conductivity with low impurity levels.

3.4 Vapor-Phase Deposition

Vapor-phase deposition refers to preparation methods such as thermal evaporation, magnetron sputtering, PLD (Pulsed laser deposition), CVD (Chemical vapor deposition), and ALD (Atomic layer deposition), in which precursors are transported to the substrate surface as vapor-phase species, plasma, or vapor reactants and then form thin-film solid electrolytes or interfacial layers under controlled atmosphere or high vacuum. Unlike ball milling, solid-state reaction, and solution synthesis, which mainly target bulk powders, vapor-phase routes emphasize thin-film formation, interfacial integration, and compatibility with microdevices. In recent years, the development of thin-film micro-batteries has shown that vapor-phase deposition can realize nanoscale thickness control, dense film construction, and conformal coating of complex three-dimensional structures, providing an important technical basis for highly integrated all-solid-state thin-film micro-batteries[81]. Among them, LiPON is one of the most representative vapor-deposited solid electrolytes and is commonly deposited by radio-frequency magnetron sputtering or PLD. It has been widely used in thin-film micro-batteries and on-chip energy-storage devices, providing an important processing reference for the preparation of halide thin-film electrolytes and interfacial layers[81—83].

In halide SSEs, the earliest and relatively systematic vapor-phase studies focused mainly on fluoride thin-film systems. As early as 1981, Oi and Miyauchi[84] prepared amorphous mLiF·nAlF$_3$ films by thermal evaporation. A mixture of LiF and AlF_3 was evaporated under a vacuum of 1 mPa and deposited onto glass substrates to form transparent amorphous films with a thickness of about 0.8 μm. When the composition satisfied $1 \leqslant m/n \leqslant 5/3$, the films exhibited ionic conductivities above 10^{-6} S/cm. Later, Oi[85] extended this strategy to mLiF-MF$_3$ (M=Al, Cr, Sc, or Al+Sc) systems, again using evaporation under 1 mPa vacuum onto glass substrates to obtain amorphous films about 0.5 μm thick. These LiF-MF$_3$ films also achieved conductivities $>10^{-6}$ S/cm. These early studies showed that fluoride thin films can form amorphous ion conductors *via* vapor evaporation and that their relatively high ion conduction may be related to locally high coordination environments in the amorphous structure. However, the literature also noted that the total conductivity in these systems may not arise solely from Li^+; proton or F^- migration may also contribute.

After ALD became an important research direction, Li-Al-F films further demonstrated the value of vapor-phase methods in interface engineering. Xie *et al.*[86] prepared $LiAlF_4$ lithium-ion-conducting interfacial layers by ALD and used them as coatings on high-voltage cathode surfaces. The $LiAlF_4$ film possessed good

ionic conductivity and a wide electrochemical stability window, outperforming single LiF or AlF_3 coatings and improving the cycling stability of Ni-rich cathodes over a wide voltage window of 2.75—4.50 V. Mäntymäki *et al.*[87] investigated conversion-type deposition of Li_3AlF_6 films. Because direct ALD of Li_3AlF_6 is difficult, they employed two conversion reactions: alternating pulses of $Al(thd)_3$ and TiF_4 onto a LiF film surface, and exposure of an AlF_3 film to Lithd (lithium 2,2,6,6-tetramethyl-3,5-heptanedionate) vapor to convert it into a Li_3AlF_6-containing film. This study showed that ternary fluoride films do not necessarily have to be obtained by direct deposition of the target phase, but can also be realized through precursor-layer conversion reactions compatible with ALD. However, LiF impurity phases, Ti contamination, and film porosity may arise. Thus, $LiAlF_4$ and Li_3AlF_6 represent two typical functional roles of vapor-phase methods in halide SSEs: the former emphasizes high-voltage cathode interfacial protection, whereas the latter focuses on constructing ternary fluoride thin-film electrolytes.

Overall, vapor-phase methods should be regarded as tools for thin-film fabrication and interface engineering rather than as bulk-material preparation routes for halide SSEs. Their advantages include dense films, precise thickness control, and strong interfacial coverage capability. Their disadvantages include expensive equipment, low deposition rates, limited precursor choices, and small throughput, making them unsuitable for large-scale powder electrolyte production. Therefore, in future halide solid-state batteries, vapor-phase methods are more likely to be applied first to high-voltage cathode coatings, microbattery electrolyte layers, and nanoscale ion-conducting protective layers at complex electrode interfaces, rather than replacing ball milling or wet-chemical routes as mainstream powder-production processes.

3.5 Other Processing Methods

In addition to ball milling, solid-state reaction, solution synthesis, and vapor-phase deposition, a series of auxiliary processes have recently been developed for SSEs, including freeze-drying, moisture/hydrate-assisted methods, ball-milling-ultrasonication coupling, and data-driven process optimization. These methods are usually not completely independent of the four routes described above, but are coupled with liquid-phase synthesis, mechanochemical processing, or electrode fabrication. They mainly address particle-size control, improved interfacial contact, enhanced air stability, construction of high-loading cathodes, and process consistency during scale-up.

As shown in Fig.8(A), freeze-drying provides an auxiliary solution-based route for regulating particle size and improving interfacial contact in halide SSEs[88]. It is essentially a combined process of liquid-phase mixing, freeze-drying, and subsequent annealing. Compared with ordinary aqueous evaporation, freeze-drying can preserve the spatial distribution of solutes after solution freezing, avoiding the formation of large particles caused by concentration gradients, local crystallization, and particle agglomeration during conventional evaporation. This method is therefore particularly suitable for preparing halide electrolyte powders with smaller and more uniform particle sizes, and for further improving ion-transport pathways and solid-solid interfacial contact in composite cathodes. In 2023, Ma *et al.*[88] first applied freeze-drying to the preparation of Li_3InCl_6 solid electrolytes. In this process, LiCl and $InCl_3$ were dissolved in deionized water in stoichiometric proportions, rapidly frozen into a solid in air, sublimation-dried to obtain hydrated precursors, and then heated at 200—400 ℃ for 4 h under vacuum to obtain Li_3InCl_6. In the resulting Li_3InCl_6, 80% of the particles were smaller than 200 nm, which is more favorable than ball milling or ordinary hydrate methods for forming continuous ion-transport networks in cathode composite layers. This work shows that the core advantage of freeze-drying is not simply to increase the intrinsic conductivity of the material, but to enhance overall ion transport in high-loading all-solid-state batteries through particle-size regulation and improved interfacial contact.

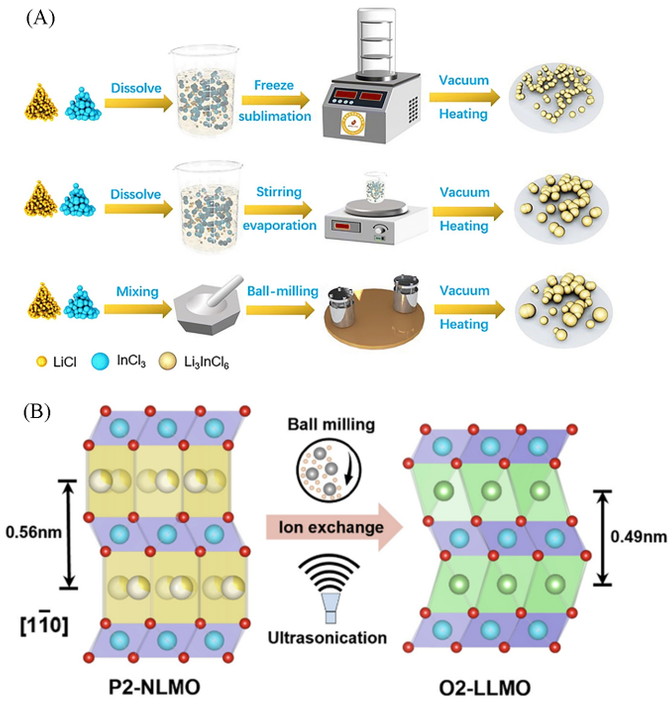


Fig. 8 Auxiliary processing routes for halide SSEs and ion-exchange-assisted structural evolution

(A) Schematic comparison of freeze-drying, hydration and ball-milling routes for preparing Li_3InCl_6 solid electrolytes[88]; (B) atomic structural evolution before and after ball-milling- or ultrasonication-assisted ion exchange[90].

(A) Copyright 2023, the Royal Society of Chemistry; (B) Copyright 2026, American Chemical Society.

Traditionally, halide SSEs have been expected to avoid moisture as much as possible because water can cause hydrolysis of halides, formation of oxide/hydroxide impurities, and decreased ionic conductivity. However, some recent studies have instead exploited controlled moisture or hydrate intermediates to construct stable structures, developing new hydrate-assisted or moisture-assisted routes. The key to these approaches is not uncontrolled exposure of electrolytes to air, but the use of H_2O/CO_2 to induce favorable surface-protective layers or intermediate phases under specific precursor compositions, humidity conditions, and post-treatment windows. Zhu *et al.*[89] prepared a Zr-based core-shell halide electrolyte, $Li_2Zr_{1.5}OCl_6@Li_2CO_3$ (LZOC-H), under industrially feasible dry-room conditions (dew point <−40 ℃). This method uses trace H_2O and CO_2 during synthesis to form a Li_2CO_3-rich outer layer *in situ*, thereby significantly improving the humid-air stability of the electrolyte. The resulting LZOC-H achieved a ionic conductivity of 1.12 mS/cm and excellent moisture tolerance. This result suggests that, for some Zr-based halide systems, appropriately using moisture and carbonate surface chemistry may be closer to practical industrial manufacturing needs than strictly anhydrous routes.

Although not directly focused on halide SSEs, Fig. 8 (B) illustrates that coupling ball milling with liquid-phase ultrasonication can provide a useful reference for low-temperature ion-exchange and metastable-structure regulation[90]. It is worth noting that Ji *et al.*[90] reported an energy-transfer-regulated Li-Na ion-exchange mechanism in layered oxide cathodes and compared ball milling and liquid-phase ultrasonication exchange routes. Ball milling can rapidly introduce defects and promote ion migration through mechanical impact, but it can also cause local structural damage. Liquid-phase ultrasonication better preserves the integrity of the layered structure, although its reaction kinetics are relatively slow. On this basis, the authors further proposed a sequential ball-milling-ultrasonication process, in which short-time ball milling first provides structural pre-activation and defect introduction, followed by an ultrasonication-assisted liquid-phase

process to complete ion exchange. This enabled 98.3% Li-Na exchange within 2 h while maintaining good structural integrity. Although this work focused on layered oxide cathodes rather than halide SSEs, its concept of using ball milling to provide structural activation energy and then using liquid-phase/ultrasonication processes to achieve mild ion exchange can provide a reference for multi-cation substitution, mixed-anion regulation, and metastable-structure construction in future halide systems. In particular, for some halide materials with narrow thermal-stability windows or easy volatilization at high temperature, ball-milling-ultrasonication coupling may serve as a low-temperature, rapid, and relatively structure-preserving auxiliary synthesis method, although its applicability in halide frameworks still needs further validation.

As the number of preparation parameters for halides continues to increase, traditional one-factor-at-a-time trial-and-error methods are no longer efficient for identifying optimal process windows. Data-driven methods, orthogonal experimental design, and machine-learning models have begun to be introduced into the preparation of halide SSEs. Beltran *et al.*[65] used low-cost Li_2ZrCl_6 as a model system, evaluated six key parameters in mechanochemical synthesis by orthogonal experimental design, and combined multiple linear regression with Gaussian process regression to analyze their effects on ionic conductivity. The results showed that the most important parameters affecting Li_2ZrCl_6 conductivity are the ball-to-powder ratio, milling step time, and milling speed. Structural characterization also revealed that a high-impedance intermediate spinel-LZC phase limits the material performance. Although this work still focused on ball milling, it essentially belongs to data-driven process optimization. In the future, this approach can be further extended to solution synthesis, freeze-drying, moisture-assisted processing, and dry-film formation, for example by establishing freeze-drying models linking precursor concentration, freezing rate, particle size, and conductivity, or moisture-assisted models linking dew point, water content, surface protective layers, and humid-air stability. For industrialization, the value of data-driven methods lies in improving batch-to-batch consistency, reducing blind trial and error, and providing predictable parameter windows for scale-up.

It should also be noted that the preparation route of halide SSE powders affects not only their intrinsic ionic conductivity, but also their processing compatibility in composite cathodes. For composite cathodes, the particle-size distribution, dispersibility, and surface state of electrolyte powders influence the construction of ion-transport networks and solid-solid interfacial contact among cathode active materials. Recent studies on halide catholytes have shown that particle size becomes particularly important under high cathode active material loading or high-rate cycling conditions[91]. Ball milling can reduce the particle size of halide catholytes and promote mechanochemical reactions, which may improve powder contact and facilitate Li^+ transport in composite cathodes[42,91]. At the same time, the final powder properties are sensitive to milling parameters such as ball-to-powder ratio, milling time and milling speed, indicating that particle dispersion, possible contamination and batch-to-batch consistency should be carefully controlled during process scale-up[65]. In contrast, solution-based and freeze-drying routes are more favorable for obtaining compositionally homogeneous powders with smaller particle sizes and better dispersibility. For example, freeze-dried Li_3InCl_6 with 80% of its particles smaller than 200 nm can improve charge transport and overall interfacial contact in composite cathodes[88]. In addition, Li_3InCl_6 has been used in slurry-coated $LiNi_{0.8}Co_{0.1}Mn_{0.1}O_2$ composite cathodes, indicating its potential compatibility with wet electrode processing and interfacial-stability optimization[92]. Therefore, future process optimization of halide SSEs should consider not only powder ionic conductivity, but also particle morphology, surface chemistry, dispersibility, and compatibility with dry or wet composite-cathode fabrication.

As shown in Fig.9, which provides a qualitative comparison based on the reviewed literature and process characteristics discussed above, ball milling remains the most commonly used method for laboratory

exploration of halide SSEs. It is suitable for rapid screening of new compositions and construction of disordered structures, but its batch consistency, energy consumption, and scale-up stability still need optimization[46,65]. The solid-state route has the highest value for structural confirmation and is suitable for studying standard phases, metastable phases, and phase-diagram relationships, but long heat treatments and sealed-atmosphere control make it difficult to serve as a high-throughput and low-cost preparation route. Solution synthesis combines low temperature, homogeneous mixing, and potential continuous processing, and has shown good scale-up potential especially in systems such as Li_3InCl_6, making it one of the most noteworthy scalable routes[37,77]. Although vapor-phase deposition is not suitable for powder electrolyte production, it is irreplaceable for thin-film microbatteries and high-voltage cathode interface protection[81,86]. Auxiliary methods such as freeze-drying, moisture-assisted processing, and dry-film formation are closer to device-manufacturing requirements and are particularly beneficial for high-loading composite cathodes, dry-room compatibility, and electrode/electrolyte interfacial integration[88,89]. Therefore, future industrialization of halide electrolytes will likely not rely on a single preparation route, but rather on an integrated manufacturing mode involving solution/mechanical powder production, dry or wet electrode integration, and data-driven process optimization.

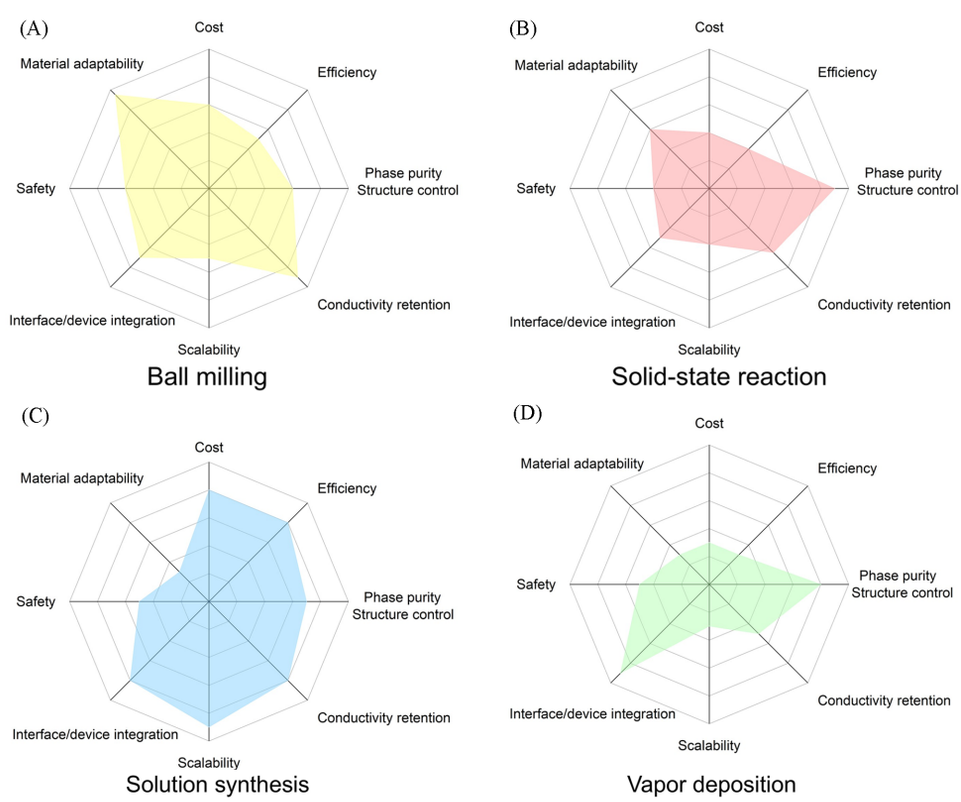


Fig. 9 Qualitative comparison of representative preparation strategies and scale-up pathways for halide SSEs

4 Future Perspectives and Commercialization Analysis

Halide SSEs have evolved from early exploration of single high-conductivity materials toward the stage of material design, process manufacturing, and industrial scale-up. Compared with sulfide and oxide systems, halide SSEs combine high oxidative stability, favorable cathode interfacial compatibility, and certain mechanical compressibility, giving them clear advantages on the high-voltage cathode side[37,44—46]. However, the transition from laboratory materials to practical batteries still faces a series of issues, including insufficient low-cost material systems, sensitivity to moisture, limited interfacial stability against Li-metal anodes, and

immature scalable preparation[46]. Therefore, the future development of halide SSEs should not focus only on higher conductivity, but should systematically optimize material cost, preparation process, interfacial stability, and industrial manufacturing.

4.1 Expansion of New Material Systems

Future development of new halide SSEs should shift from single-performance optimization toward comprehensive-property optimization. Early high-performance halides were mainly concentrated in materials such as Li_3YCl_6, Li_3YBr_6, Li_3InCl_6, and Li_3ScCl_6 which have demonstrated that halides can achieve ionic conductivities on the order of 10^{-3} S/cm or even higher[37,44,45]. From an industrialization perspective, however, elements such as Y, In and Sc still face limitations in cost and resource supply, so low-cost, rare-earth-free, or rare-earth-lean systems will become important directions for future development[46]. For example, chloride, oxyhalide, and nitride-halide systems involving Zr, Mg, and Al have already shown promise, among which Zr-based oxychlorides and nitride-chlorides combine relatively high ionic conductivity with a more favorable cost basis[47—49,55,58].

More broadly, future material design should consider not only the properties after synthesis, but also whether the material is compatible with scalable preparation processes from the outset. For example, Li_3InCl_6, as a relatively mature representative system for solution synthesis, is attractive not only because of its high ionic conductivity and air stability, but also because it can undergo controllable hydration/dehydration transitions and can be prepared at low temperature *via* water-mediated or organic-solvent routes[74,78,93]. Therefore, more solution-friendly halide materials could be designed in the future, namely material systems that do not undergo irreversible hydrolysis easily, can form stable hydrate/solvate intermediates, and can recover highly conductive phases during low-temperature desolvation.

In addition, reaction-pathway design for rapid synthesis should be emphasized, that is, selecting precursors with higher reactivity, shorter diffusion paths, or "catalytic" effects to shorten conventional long-time milling or annealing processes. For example, as shown in Fig.10(A), the XRD patterns of pristine and 18 min ball-milled Li_2ZrCl_6 demonstrate the rapid structural evolution during ultrafast ball milling, indicating that reaction-pathway design can greatly shorten the synthesis time of Zr-based oxyhalide Li_2ZrCl_6 (oh-LZC)[94]. The oh-LZC phase can be obtained within 18 min, and its conductivity increases to 1.09 mS/cm after extending the milling time to 1.5 h, as supported by the EIS results in Fig.10(B)[94]. The SEM images further show the morphological evolution of Li_2ZrCl_6 before and after ball milling[Fig.10(C) and (D)], while the schematic illustration in Fig.10(E) describes the formation of Li_2ZrCl_6 and the evolution of amorphous three-dimensional Li^+ transport channels during milling. This work used Ta_2O_5 instead of Li_2O as a low-cost oxygen source and proposed that Ta_2O_5 acts as a core-like pseudo-catalyst during ball milling to promote the formation of a conductive amorphous oxyhalide shell, providing a new materials-design concept for minute-scale synthesis of halide SSEs. In addition, amorphous $LiTaOCl_4$ can also be synthesized within about 4 h through a two-step rapid reaction route and exhibits good cycling performance in all-solid-state batteries over a wide temperature range and at high rates. This suggests that material systems capable of rapidly forming highly ion-conductive amorphous networks may be more suitable for future large-scale manufacturing[72].

Therefore, the evaluation criteria for future halide materials should expand beyond ionic conductivity to include low-cost raw materials, dry-room-compatible processing, cathode/anode interfacial stability, compressibility, compatibility with high-loading cells, and friendliness to process scale-up. For materials intended for practical batteries, high conductivity alone is not sufficient for commercialization; the material system must also satisfy manufacturability and supply-chain sustainability requirements[46].

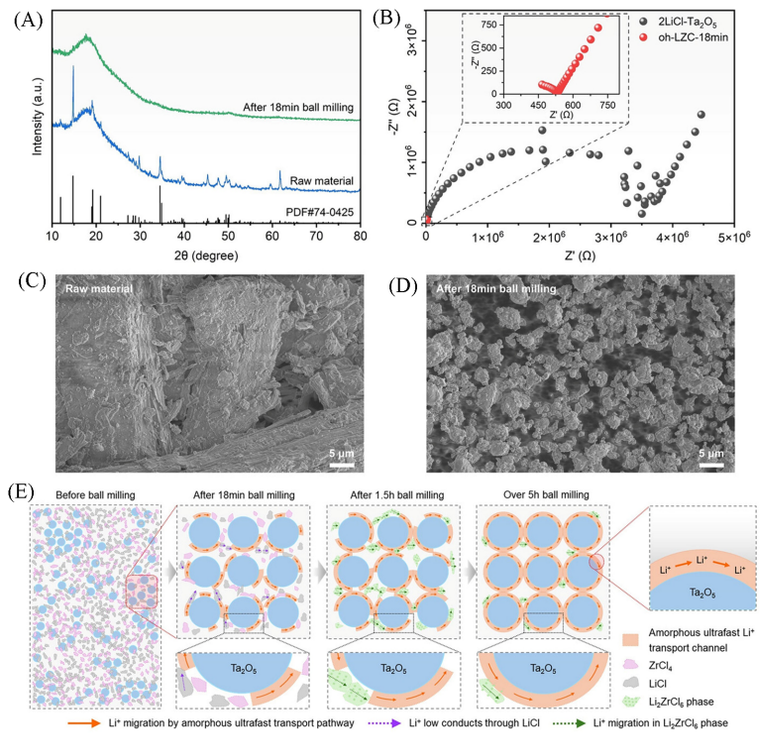


Fig. 10 Ball-milling-induced structural evolution of oh-LZC[94]

(A) XRD patterns of pristine and 18 min ball-milled $ZrCl_4$; (B) EIS spectra of oh-LZC-18 min and 2LiCl-Ta_2O_5 samples; (C, D) SEM images of pristine and 18 min ball-milled $ZrCl_4$; (E) schematic illustration of Li_2ZrCl_6 formation and amorphous 3D Li^+ transport-channel evolution during ball milling.

Copyright 2025, Wiley-VCH.

4.2 Process-Route Optimization

The preparation of halide SSEs has expanded from ball milling, solid-state annealing, and solution synthesis to vapor-phase deposition, freeze-drying, and intelligent-assisted routes. The key in the future is not simply to choose a single "best" method, but to match the most appropriate process route to the material attributes. For example, ball milling is suitable for rapid screening of new compositions and for inducing amorphization, but it must address nonuniform energy transfer, batch-to-batch consistency, and moisture control during scale-up. The solid-state route is suitable for structural confirmation and standard-sample preparation, but requires long reaction times and demanding sealing conditions. Solution synthesis has low-temperature, homogeneous-mixing, and continuous-processing potential, but must solve problems such as material hydrolysis, solvent residue, and controlled dehydration. Vapor-phase methods are more suitable for ultrathin interfacial layers and microdevices, but not for large-scale powder production[37,44—46].

From the perspective of process optimization, future ball-milling routes should move from empirical long-duration milling toward parameterized, short-process, and scalable milling. Existing studies show that the ball-to-powder ratio, milling step time, and milling speed significantly affect the phase structure and final ionic conductivity of Li_2ZrCl_6, and the optimal process window can therefore be identified through orthogonal experimental design, regression models, and machine-learning methods[65]. Rapid mechanochemical synthesis is also worth attention. For example, Zr-based oxyhalide oh-LZC can form a conductive phase through 18 min ultrafast ball milling, indicating that precursor reaction-pathway design and optimized equipment energy input may significantly shorten synthesis time[94]. In the future, combining such efficiency-optimized systems with continuous ball mills, vibration mills, stirred mills, or industrial horizontal ball-milling equipment could reduce the time cost and energy consumption of halide powder production.

In addition, process-route optimization should also include equipment modification and process monitoring. Laboratory planetary milling, glovebox sealing, and small-batch vacuum drying cannot be directly translated to industrial manufacturing. In response to the moisture sensitivity and corrosiveness of halides, future work should develop sealed continuous-feeding and discharging milling equipment, low-dew-point dry-room continuous mixing systems, controllable desolvation reactors, and online detection technologies for powder particle size, moisture, and phase composition. Especially for solution synthesis, residual moisture, desolvation rate, and intermediate-phase transformation significantly influence the final structure and conductivity; therefore, real-time monitoring and closed-loop control will be essential for improving batch consistency. Overall, the commercial manufacturing of future halide solid-state batteries will likely not rely on a single process route, but on a coupled multi-process manufacturing mode in which material design is adapted to the process and the process in turn screens materials.

4.3 *In Situ* Characterization

The performance of halide SSEs is highly dependent on local structure, degree of amorphization, and interfacial reactions. Conventional *in situ* XRD (X-ray diffraction) or electrochemical tests alone are insufficient to fully elucidate their formation mechanisms and failure processes. Therefore, more advanced characterization techniques, including synchrotron XRD, PDF(Pair distribution function), solid-state NMR (Nuclear magnetic resonance), *in situ* Raman spectroscopy, neutron diffraction, and neutron PDF, should be introduced in future studies[66,74,78,93,95,96].

Among these methods, neutron-related characterization has special significance for halide SSEs. Because Li scatters X-rays weakly, and because halide systems often contain Li^+/metal-cation site disorder, vacancy distributions, stacking faults, and local structural distortions, neutron diffraction is more effective for resolving Li^+ site occupancy, defect distributions, and the degree of cation disorder. Combined with neutron PDF analysis, it can also provide short-range-order information in amorphous or nanocrystalline systems. Therefore, neutron characterization can be used not only to determine average crystal structures, but also to correlate local structures, anion dynamics, and ion-transport mechanisms[75,95,96].

During material formation, *in situ* synchrotron XRD and neutron diffraction can track solid-state reactions, annealing-induced phase transitions, and metastable-phase formation. For example, studies on the solid-state formation of β-Li_3YCl_6 have shown that the temperature window has a decisive influence on metastable-phase formation[66]. Sebti *et al.*[50] revealed the relationship between stacking faults and Li^+ migration in Li_3YCl_6 through neutron diffraction and simulations, demonstrating the important role of neutron diffraction in resolving Li^+ sites, defect structures, and transport channels in halides. Brahmbhatt *et al.* [75] compared aqueous ammonium-assisted synthesis, ammonium-free aqueous synthesis, and mechanically mixed routes for Li_3YCl_6 using *in situ* neutron diffraction, proving that intermediate-phase evolution is critical for target-phase formation. Meanwhile, Ni *et al.* [95] discussed ion-transport mechanisms in solid conductors from the dual perspective of static structural features and anion dynamics(Fig.11). As shown in Fig.11(A)—(C), neutron diffraction refinements reveal the temperature and composition-dependent structural evolution of Li_2ODCl and Li_2ODBr, including the transition of Li_2ODCl from orthorhombic *Pban* at 300 K to cubic $Pm\bar{3}m$ at 400 K. The refined structures in Fig.11(D)—(F) further show the distribution of Li, O, D, halogen atoms and vacancies in Li_2ODX(X=Cl, Br), highlighting the role of neutron characterization in correlating crystal structure, anion dynamics and ion transport. For ball-milled systems, future studies can combine time-resolved neutron diffraction, PDF, and solid-state NMR to investigate the transformation pathway from precursors to amorphous/nanocrystalline phases during milling, answering key questions such as how long the reaction takes, when beneficial defects are generated, and whether over-milling causes structural degradation. For amorphous

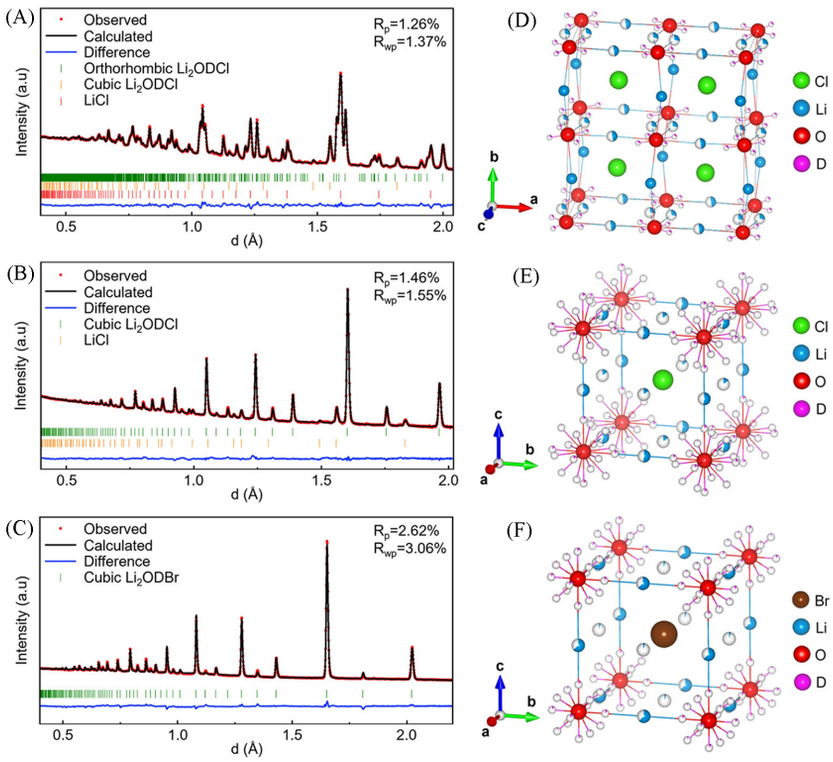


Fig. 11 Neutron diffraction refinements and crystal structures of Li_2ODX(X=Cl, Br)[95]

(A) Rietveld refinement of Li_2ODCl at 300 K in the orthorhombic *Pban* space group; (B) Rietveld refinement of Li_2ODCl at 400 K in the cubic $Pm\bar{3}m$ space group; (C) Rietveld refinement of Li_2ODBr at 300 K in the cubic $Pm\bar{3}m$ space group; (D—F) refined crystal structures of Li_2ODX(X=Cl, Br).

Copyright 2025, American Chemical Society.

multi-anion systems such as oxyhalides and nitride-halides, neutron PDF can also reveal short-range coordination environments inaccessible to conventional XRD, providing complementary evidence for understanding O^{2-}- or N^{3-}-induced amorphization, local polyhedral reconstruction, and the formation of continuous Li^+ transport networks.

Real-time characterization not only helps reveal mechanisms but can also guide process optimization. For example, in solution synthesis, *in situ* Raman spectroscopy, NMR, and synchrotron techniques can be used to track the evolution of hydrates, ammonium salt intermediates, and dehydration products[74,78,93]. In freeze-drying and moisture-assisted processes, these methods can clarify the relationships among freezing rate, water content, and the formation of surface protective layers[88,89]. In vapor-phase deposition, *in situ* ellipsometry and microbalance measurements can monitor ALD growth rates and film compositions.

4.4 AI-Assisted Optimization

Halide SSEs possess an extremely large compositional space. Taking the Li-M-X system as an example, the M-site cations can cover rare-earth, transition-metal, and main-group elements, while the X site can include Cl, Br, I and F. Non-halide anions such as O^{2-} and N^{3-} can be further introduced. Traditional trial-and-error methods are inefficient for screening such a vast materials space; therefore, AI for science, machine learning, and high-throughput computation are expected to play increasingly important roles in future halide research.

For new material discovery, machine learning can be used to predict key descriptors such as phase stability, ionic conductivity, redox stability window, elastic modulus, and air stability. Combined with first-principles calculations, molecular dynamics, and crystal-structure databases, it can rapidly screen

low-cost candidate materials with high conductivity and wide electrochemical windows. For amorphous oxyhalides and nitride-halides, conventional crystal-structure databases are not fully applicable; therefore, graph neural networks, active learning, and generative models targeting amorphous structures should be developed to predict local coordination environments, network connectivity, and Li^+ diffusion barriers.

AI is equally important for process optimization. Beltran *et al.* [65] have applied orthogonal experimental design, multiple linear regression, and Gaussian process regression to optimize parameters for the mechanochemical synthesis of Li_2ZrCl_6, identifying the ball-to-powder ratio, milling step time, and milling speed as key factors affecting conductivity. This concept can be extended in the future to solution synthesis, freeze-drying, and solid-state annealing. For example, models can be built for "milling speed-milling time-ball-to-powder ratio-phase purity-conductivity", or for liquid-phase synthesis linking "solvent type-precursor concentration-dehydration temperature-oxygen contamination-conductivity". Through active learning, the optimal process window can be rapidly determined with the fewest experiments, improving batch consistency and scale-up efficiency. A more ideal future direction is to establish materials-process-structure-property databases in which synthesis parameters, structural characterization, electrochemical performance, and failure data are standardized in a unified manner.

4.5 Commercialization Analysis

From the perspective of current industrial progress, halide SSEs have not yet established a clear large-scale full-cell industrial route comparable to those of sulfide, oxide, or polymer systems. Publicly available signs of halide commercialization are mainly concentrated at two levels: first, halide powders such as Li_3InCl_6 and Li_3YCl_6 have entered research-grade and small-batch supply; second, industry-academia-research projects such as HELENA have begun full-cell validation of halide solid-state batteries. Thus, halides are transitioning from laboratory materials toward pilot-scale validation and specific application scenarios.

From the material-supply side, Li_3InCl_6 is one of the halide SSEs showing relatively clear signs of commercialization. Xnergy Materials has publicly sold Li_3InCl_6 powder and provides coarse- and fine-particle grades, with nominal ionic conductivities of >1.4 and >1.0 mS/cm, respectively, positioning it as a cathode-side electrolyte for high-voltage oxide cathodes and as a base material for halide research. Such products indicate that halide powders have moved from literature materials to research procurement and small-batch validation, although their specifications remain mainly R&D-grade or small-batch products and cannot yet be regarded as a mature ton-scale battery-material supply chain. The European HELENA project is a representative case explicitly targeting halide solid-state batteries. According to CORDIS, the full name of HELENA is "Halide solid state batteries for ELectric vEhicles aNd Aircrafts". Coordinated by CIC energiGUNE and supported by Horizon Europe with a total budget of about 8.367 million euros, the project aims to develop high-energy solid-state batteries based on high-capacity lithium-metal anodes, Ni-rich NMC cathodes, and superionic halide SSEs. Project progress shows that HELENA has prepared laboratory cells with areal capacities up to about 4 $mA\cdot h/cm^2$ using NMC622, halide electrolytes, and unprotected Li-metal anodes. CIC energiGUNE further reported that the project has assembled the first complete cells using halide electrolytes and validated conductivities at the several mS/cm level, dry-room operability, thermal stability, and voltage stability. In addition, the HELENA project disclosed a patent application by Saint-Gobain Recherche related to interfacial stability of halide electrolytes, indicating that this direction has begun to move from materials validation toward interface engineering and intellectual-property deployment.

For halides to move further toward commercialization, key issues such as low-cost raw-material systems,

dry-room-compatible processing, stable kilogram- to ton-scale supply, high-areal-loading composite cathode manufacturing, and long-term interfacial stability still need to be addressed.

5 Summary and Outlook

In this review, the recent progress in preparation strategies of halide SSEs has been summarized from the perspectives of material systems, synthetic routes, structural evolution, and scale-up potential. The development of halide SSEs demonstrates that high ionic transport in halide SSEs is closely related to anion-framework arrangement, cation disorder, defect chemistry, and amorphization. More importantly, these structural features are strongly affected by the preparation route. Ball milling, solid-state reaction, solution synthesis, vapor-phase deposition, and hybrid processing strategies not only determine phase formation and local structure, but also influence particle morphology, interfacial contact, batch reproducibility, and manufacturability.

Despite the rapid progress, the practical application of halide SSEs still faces several challenges. First, many high-performance systems rely on expensive or moisture-sensitive raw materials, making cost reduction and moisture stability critical issues. Second, current laboratory-scale methods cannot be directly translated into large-scale manufacturing, because process parameters such as atmosphere, residual solvent, milling energy, heat-treatment window, and drying conditions have strong effects on phase purity and ionic conductivity. Third, the relationship among preparation process, local structure, interfacial evolution, and cell-level performance remains insufficiently understood, especially for amorphous oxyhalides, nitride-halides, and composite electrodes.

Future research should therefore focus on the coordinated optimization of material design, process engineering, and device-level integration. From the materials perspective, low-cost, rare-earth-lean, or rare-earth-free compositions need to be further developed to reduce raw-material cost and improve the feasibility of large-scale production. At the same time, moisture stability, interfacial compatibility with high-voltage cathodes and Li-metal or alloy anodes, and mechanical processability should be considered together with ionic conductivity, rather than being treated as separate optimization targets. From the processing perspective, reproducible and scalable routes such as continuous mechanochemical synthesis, controllable solution processing, freeze-drying, dry-electrode fabrication, and vapor-phase interface modification should be systematically explored. Particular attention should be paid to the relationships between preparation parameters, phase formation, particle morphology, surface chemistry, and composite-electrode compatibility, which directly determine whether halide SSEs can move from laboratory-scale powder synthesis to practical battery manufacturing.

In addition, deeper mechanistic understanding and more reliable process control are still required. Advanced characterization techniques, including synchrotron XRD, neutron diffraction, PDF, solid-state NMR, and *in situ* Raman spectroscopy, can provide multiscale information on average structures, local coordination environments, ion-transport pathways, and interfacial evolution. When combined with high-throughput experiments, machine-learning models, and process databases, these techniques are expected to reveal the formation and failure mechanisms of halide SSEs and establish quantitative materials-process-structure-property relationships. Such knowledge would help identify predictable synthesis windows, improve batch-to-batch consistency, and accelerate the scale-up of promising halide electrolyte systems. These insights may not only promote the practical application of halide SSEs in all-solid-state lithium batteries, but also provide useful guidance for developing solid electrolytes in other emerging metal-battery systems, such as Na-, Cu-, and Ag-based electrolytes.

The authors thank Shenzhen Guangming Science City Development and Construction Co., Ltd. and its Material Genome Big-Science Facilities Platform.

References

[1] Dunn B., Kamath H., Tarascon J. M., *Science*, **2011**, *334*, 928—935
[2] Armand M., Tarascon J. M., *Nature*, **2008**, *451*, 652—657
[3] Goodenough J. B., Park K. S., *J. Am. Chem. Soc.*, **2013**, *135*, 1167—1176
[4] Grey C. P., Hall D. S., *Nat. Commun.*, **2020**, *11*, 6279
[5] Albertus P., Babinec S., Litzelman S., Newman A., *Nat. Energy*, **2018**, *3*, 16—21
[6] Liu J., Bao Z. N., Cui Y., Dufek E. J., Goodenough J. B., Khalifah P., Li Q. Y., Liaw B. Y., Liu P., Manthiram A., Meng Y. S., Subramanian V. R., Toney M. F., Viswanathan V. V., Whittingham M. S., Xiao J., Xu W., Yang J. H., Yang X. Q., Zhang J. G., *Nat. Energy*, **2019**, *4*, 180—186
[7] Li M., Lu J., Chen Z. W., Amine K., *Adv. Mater.*, **2018**, *30*, 1800561
[8] Grey C. P., Tarascon J. M., *Nat. Mater.*, **2017**, *16*, 45—56
[9] Janek J., Zeier W. G., *Nat. Energy*, **2016**, *1*, 16141
[10] Bachman J. C., Muy S., Grimaud A., Chang H. H., Pour N., Lux S. F., Paschos O., Maglia F., Lupart S., Lamp P., Giordano L., Shao-Horn Y., *Chem. Rev.*, **2016**, *116*, 140—162
[11] Manthiram A., Yu X. W., Wang S. F., *Nat. Rev. Mater.*, **2017**, *2*, 16103
[12] Famprikis T., Canepa P., Dawson J. A., Islam M. S., Masquelier C., *Nat. Mater.*, **2019**, *18*, 1278—1291
[13] Xiao Y., Wang Y., Bo S. H., Kim J. C., Miara L. J., Ceder G., *Nat. Rev. Mater.*, **2020**, *5*, 105—126
[14] Banerjee A., Wang X. F., Fang C. C., Wu E. A., Meng Y. S., *Chem. Rev.*, **2020**, *120*, 6878—6933
[15] Schnell J., Günther T., Knoche T., Vieider C., Köhler L., Just A., Keller M., Passerini S., Reinhart G., *J. Power Sources*, **2018**, *382*, 160—175
[16] Janek J., Zeier W. G., *Nat. Energy*, **2023**, *8*, 230—240
[17] Schmaltz T., Hartmann F., Wicke T., Weymann L., Neef C., Janek J., *Adv. Energy Mater.*, **2023**, *13*, 2301886
[18] Ma M. M., Zhang M. H., Jiang B. T., Du Y., Hu B. C., Sun C. G., *Mater. Chem. Front.*, **2023**, *7*, 1268—1297
[19] Ohno S., Banik A., Dewald G. F., Kraft M. A., Krauskopf T., Minafra N., Till P., Weiss M., Zeier W. G., *Prog. Energy*, **2020**, *2*, 022001
[20] Fu Z. H., Chen X., Yao N., Yu L. G., Shen X., Zhang R., Zhang Q., *Chem. J. Chinese Universities*, **2023**, *44*(5), 20220703
[21] Zhang Y., Chen Y. T., Shi J. Y., Huang K. K., *Chin. J. Appl. Chem.*, **2024**, *41*(4), 484—495
[22] Chen Y. T., Feng Y., Ren Y., Huang K. K., *EnergyChem*, **2025**, *7*(3), 100157
[23] Zhang Z., Shao Y. J., Lotsch B., Hu Y. S., Li H., Janek J., Nazar L. F., Nan C. W., Maier J., Armand M., Chen L. Q., *Energy Environ. Sci.*, **2018**, *11*, 1945—1976
[24] Zhao Q., Stalin S., Zhao C. Z., Archer L. A., *Nat. Rev. Mater.*, **2020**, *5*, 229—252
[25] Zhang Q., Cao D. X., Ma Y., Natan A., Aurora P., Zhu H. L., *Adv. Mater.*, **2019**, *31*, 1901131
[26] Liang J. W., Li X. N., Adair K. R., Sun X. L., *Acc. Chem. Res.*, **2021**, *54*, 1023—1033
[27] Kwak H., Wang S., Park J., Liu Y., Kim K. T., Choi Y., Mo Y., Jung Y. S., *ACS Energy Lett.*, **2022**, *7*, 1776—1805
[28] Combs S. R., Todd P. K., Gorai P., Maughan A. E., *J. Electrochem. Soc.*, **2022**, *169*, 040551
[29] Tuo K., Sun C., Liu S., *Electrochem. Energy Rev.*, **2023**, *6*, 17
[30] Tang X. H., Xie F., Lu Y. X., Rong X. H., Chen L. Q., Hu Y. S., *EES Batteries*, **2025**, *1*, 1481—1501
[31] Asano T., Sakai A., Ouchi S., Sakaida M., Miyazaki A., Hasegawa S., *Adv. Mater.*, **2018**, *30*, 1803075
[32] Li X. N., Liang J. W., Luo J., Adair K. R., Wang C., Banis M. N., Sham T. K., Sun X. L., *Energy Environ. Sci.*, **2019**, *12*, 2665—2671
[33] Park K. H., Kaup K., Assoud A., Zhang Q., Wu X. H., Nazar L. F., *ACS Energy Lett.*, **2020**, *5*, 533—539
[34] Wang K., Gu Z., Xi Z., Hu L., Wang Z., Wang J., Li H., Chen F., Ma C., *Nat. Commun.*, **2021**, *12*, 4410
[35] Kochetkov I., Zuo T. T., Ruess R., Singh B., Zhou L., Kaup K., Janek J., Nazar L. F., *Energy Environ. Sci.*, **2022**, *15*, 3933—3943
[36] Li X. N., Liang J. W., Adair K. R., Li J., Li W., Zhao F., Hu Y., Sham T. K., Zhang L., Zhao S., Lu S., Huang H., Li R., Chen N., Sun X. L., *Nano Lett.*, **2020**, *20*, 4384—4392
[37] Li X. N., Liang J. W., Yang X., Adair K. R., Wang C. H., Zhao F. P., Sun X. L., *Energy Environ. Sci.*, **2020**, *13*, 1429—1461
[38] Wang Q. D., Zhou Y. N., Wang X. L., Guo H., Gong S. P., Yao Z. P., Wu F. T., Wang J. L., Ganapathy S., Bai X. D., Li B. H., Zhao C. L., Janek J., Wagemaker M., *Nat. Commun.*, **2024**, *15*, 1050
[39] Ginnings D. C., Phipps T. E., *J. Am. Chem. Soc.*, **1930**, *52*, 1340—1345
[40] Hartwig P., Weppner W., Rabenau A., *Solid State Ionics*, **1981**, *3/4*, 249—254
[41] Schlem R., Bernges T., Li C., Mrovec M., Zobel M., Fuchs T., Schmidt D., Wilkening H. M. R., Zeier W. G., *ACS Appl. Energy Mater.*, **2020**, *3*, 3684—3691

[42] Luo X., Zhong Y., Wang X., Xia X., Gu C., Tu J., *ACS Appl. Mater. Interfaces*, **2022**, *14*, 49839—49846
[43] Liu X., Mi F., Sun C., *Chem. Commun.*, **2025**, *61*, 1144—1147
[44] Tao B., Zhong D., Li H., Wang G., Chang H., *Chem. Sci.*, **2023**, *14*, 8693—8722
[45] Nie X., Hu J., Li C., *Interdiscip. Mater.*, **2023**, *2*, 365—389
[46] Grundish N. S., *Tungsten*, **2026**, *30*,
[47] Zhang S., Zhao F., Chen J., Fu J., Luo J., Alahakoon S. H., Chang L. Y., Feng R., Shakouri M., Liang J., Zhao Y., Li X. N., He L., Huang Y., Sun X. L., *Nat. Commun.*, **2023**, *14*, 3780
[48] Hong B., Gao L., Nan P., Li Y., Liu M., Zou R., Gu J., Xu Q., Zhu J., Han S., *Angew. Chem. Int. Ed.*, **2025**, *64*, e202415847
[49] Hong B., Gao L., Zhang B., Nan P., Zhang R., Li Y., Lei Z., Liu M., Wu J., Di L., Ni H., Han S., Zhu J., *Energy Environ. Sci.*, **2026**, *19*, 241—252
[50] Sebti E., Evans H. A., Chen H., Richardson P. M., White K. M., Giovine R., Koirala K. P., Xu Y., Gonzalez-Correa E., Wang C., Brown C. M., Cheetham A. K., Canepa P., Clément R. J., *J. Am. Chem. Soc.*, **2022**, *144*, 5795—5811
[51] Schlem R., Muy S., Prinz N., Banik A., Shao-Horn Y., Zobel M., Zeier W. G., *Adv. Energy Mater.*, **2020**, *10*, 1903719
[52] Zhou L., Kwok C. Y., Shyamsunder A., Zhang Q., Wu X., Nazar L. F., *Energy Environ. Sci.*, **2020**, *13*, 2056—2063
[53] Wang H., Li Y., Tang Y., Ye D., He T., Zhao H., Zhang J., *ACS Appl. Mater. Interfaces*, **2023**, *15*, 5504—5511
[54] Liu Z., Chien P. H., Wang S., Yao Y., Li Y., Feng X., Wang H., Liu Y., Xu R., Hu Y. Y., *Nat. Chem.*, **2024**, *16*, 1584—1591
[55] Hu L., Wang J., Wang K., Gu Z., Xi Z., Li H., Chen F., Wang Y., Li Z., Ma C., *Nat. Commun.*, **2023**, *14*, 3807
[56] Dai T., Wu S., Lu Y., Yang Y., Liu Y., Chang C., Rong X., Xiao R., Zhao J., Liu Y., Wang W., Chen L., Hu Y. S., *Nat. Energy*, **2023**, *8*, 1221—1228
[57] Hong B., Gao L., Li C., Lai G., Zhu J., Huang D., Zuo Y., Yin W., Sun M., Zhao S., Zheng J., Han S., Zou R., *Nat. Commun.*, **2025**, *16*, 143
[58] Wu T. T., Guo S. J., Zhang H. S., Jiang Y., Wang J., Zhu J., Zhang X., Wei P., Hu Z., Gao R., Chen G. H., Wen R., Wang X., Cao A. M., *Angew. Chem. Int. Ed.*, **2025**, *64*, e202510359
[59] Balaish M., Kim K. J., Chu H., Zhu Y., Gonzalez-Rosillo J. C., Kong L., Paik H., Weinmann S., Hood Z. D., Hinricher J., Miara L. J., Rupp J. L. M., *Chem. Soc. Rev.*, **2025**, *54*, 8925—9007
[60] Gombotz M., Wilkening H. M. R., *ACS Sustain. Chem. Eng.*, **2021**, *9*, 743—755
[61] Wang K., Gu Z., Xi Z., Hu L., Ma C., *Nat. Commun.*, **2023**, *14*, 1396
[62] Shi J., Yao Z., Xiang J., Cai C., Tu F., Zhang Y., Yao W., Jia Q., Zhou Y., Shen S., Sun C., *ACS Sustain. Chem. Eng.*, **2024**, *12*(5), 2009—2017
[63] Goldmann B. A., Rosenbach C., Evans H. A., Helm B., Wankmiller B., Maus O., Suard E., Nazar L. F., Hansen M. R., Morgan B. J., Islam M. S., Zeier W. G., *Chem. Mater.*, **2025**, *37*(24), 9858—9868
[64] Long Z., Hu K., *Energy Storage Mater.*, **2026**, *88*, 105136
[65] Beltran M., Wang B., Tan Y., Hsu H. Y., Lee J., Zhong D., Ceder G., *ACS Mater. Lett.*, **2026**, *8*, 614—620
[66] Ito H., Shitara K., Wang Y., Fujii K., Yashima M., Goto Y., Moriyoshi C., Rosero-Navarro N. C., Miura A., Tadanaga K., *Adv. Sci.*, **2021**, *8*, 2101413
[67] Ito H., Nakahira Y., Ishimatsu N., Goto Y., Yamashita A., Mizuguchi Y., Moriyoshi C., Toyao T., Shimizu K., Oike H., Enoki M., Rosero-Navarro N. C., Miura A., Tadanaga K., *Bull. Chem. Soc. Jpn.*, **2023**, *96*, 1262—1268
[68] Molaiyan P., Mailhiot S. E., Voges K., Kantola A. M., Hu T., Michalowski P., Lassi U., Karppinen M., Lundström M., *Mater. Des.*, **2023**, *227*, 111690
[69] Singh B., Wang Y., Liu J., Bazak J. D., Shyamsunder A., Nazar L. F., *J. Am. Chem. Soc.*, **2024**, *146*, 17158—17169
[70] Jeon S., Park K. H., Cho W., Jeong G., Yu J., Park Y. J., Kim K. S., *Solid State Ionics*, **2025**, *421*, 116791
[71] Bao H. T., Cao B. Q., Shao G. Q., *Crystals*, **2025**, *15*, 475
[72] Li L., Jiang Z., Yang J., Liu C., Luo Q., Li S., Zhang L., Chen X., Cheng S., Yu C., *Adv. Funct. Mater.*, **2025**, *35*(1), 2410008
[73] Li X., Liang J., Chen N., Luo J., Adair K. R., Wang C., Banis M. N., Sham T. K., Zhang L., Zhao S., Lu S., Huang H., Li R., Sun X., *Angew. Chem. Int. Ed.*, **2019**, *58*, 16427—16432
[74] Wang C., Liang J., Luo J., Li X. N., Sun Q., Adair K. R., Zhao F., Banis M. N., Sham T. K., Sun X. L., *Sci. Adv.*, **2021**, *7*, eabh1896
[75] Brahmbhatt T., Li C., Garaga M. N., Tsai W. Y., Greenbaum S. G., Nanda J., Sacci R. L., *Inorg. Chem. Front.*, **2024**, *11*, 3001—3010
[76] Liu H. W., Lin C. C., Chang P. Y., Haw S. C., Sheu H. S., Chen J. M., Chen C. C., Jeng R. J., Wu N. L., *J. Solid State Electrochem.*, **2022**, *26*, 1885—1896
[77] Wen S., Sheng H., Zhang Y., Zheng S., Wang Z., *J. Alloys Compd.*, **2024**, *984*, 173973
[78] Bonsu J. O., Bhadra A., Kundu D., *Adv. Sci.*, **2024**, *11*, 2403208
[79] Xiong R., Yuan L., Song R., Hao S., Ji H., Cheng Z., Zhang Y., Jiang B., Shao Y., Li Z., Huang Y., *ACS Appl. Mater. Interfaces*, **2024**, *16*, 36281—36288
[80] Rosa C., Pesce A., Lannelongue P., Ravalli M., López del Amo J. M., López-Aranguren P., Quartarone E., Tealdi C., *J. Phys. Chem. Solids*, **2026**, *209*, 113327

[81] Zheng M., Xu X., Wang X., Lin H., Hou C., Khan M., Zhu J., Han S., *Nano-Micro Lett.*, **2026**, *18*, 159
[82] Xu F., Dudney N. J., Veith G. M., Kim Y., Erdonmez C., Lai W., Chiang Y. M., *J. Mater. Res.*, **2010**, *25*, 1507—1515
[83] Zhao S. L., Fu Z. W., Qin Q. Z., *Thin Solid Films*, **2002**, *415*(1/2), 108—113
[84] Oi T., Miyauchi K., *Mater. Res. Bull.*, **1981**, *16*, 1281—1289
[85] Oi T., *Mater. Res. Bull.*, **1984**, *19*, 1343—1348
[86] Xie J., Sendek A. D., Cubuk E. J., Zhang X., Lu Z., Gong Y., Wu T., Shi F., Liu W., Reed E. J., Cui Y., *ACS Nano*, **2017**, *11*, 7019—7027
[87] Mäntymäki M., Mizohata K., Heikkilä M. J., Räisänen J., Ritala M., Leskelä M., *Thin Solid Films*, **2017**, *636*, 26—33
[88] Ma T., Wang Z., Wu D., Lu P., Zhu X., Yang M., Peng J., Chen L., Li H., Wu F., *Energy Environ. Sci.*, **2023**, *16*, 2142—2152
[89] Zhu X., Liu C., Yan X., Yue J., Zhang M., Zhang S., Wang Y., Wu H., Gong Y., Wu Y., Wang X., Xia S., Wang S., Wang Z., Zhao C., Liang J., Han S., Sun X., Li X., *Natl. Sci. Rev.*, **2026**, *13*, nwag209
[90] Ji P., Zhang L., Gan L., Zhang S., Li Y., Wang J., Lei X., Ge M., Wang L., Guo S., Guo Y., Wang W., Ma X., Wang Y., Zhang L., Wang X., Gu L., Cao A., Guo Y., Fu M., Su D., *J. Am. Chem. Soc.*, **2026**, *148*(18), 16478—16487
[91] Shen F., McGahan M., Pietras J. D., Doeff M. M., Battaglia V. S., Tucker M. C., *J. Power Sources*, **2025**, *640*, 236709
[92] Ye Q., Li X., Cheng F., Li H., Hu Y., Li X., Ma J., Li Y., *ACS Appl. Mater. Interfaces*, **2023**, *15*, 18878—18887
[93] Sacci R. L., Bennett T. H., Drews A. R., Anandan V., Kirkham M. J., Daemen L., Nanda J., *J. Mater. Chem. A*, **2021**, *9*, 990—996
[94] Zhang Y., Meng Q., Zeng A., Qiu S., Zhang H., Zhao E., Xiao X., *Angew. Chem. Int. Ed.*, **2026**, *65*, e202516259
[95] Ni H. J., Gao L., Zhu J. L., Huang D. B., Yin W., Zou R. Q., Li C. P., Han S. B., *Chem. Mater.*, **2025**, *37*(1), 278—289
[96] Dong Y., Shi H., Li H., Wu X., Jiang W., Cui W., Niu J., Xu Z., *J. Mater. Chem. A*, **2024**, *12*, 22458—22486

(Ed.: Y, K, V)